

**NASA  
Technical  
Paper  
2832**

**AVSCOM  
Technical  
Paper  
88-B-001**

1988

Effect of Advanced  
Rotorcraft Airfoil  
Sections on the Hover  
Performance of a  
Small-Scale Rotor Model

Susan L. Althoff  
*Aerostructures Directorate  
USAARTA-AVSCOM  
Langley Research Center  
Hampton, Virginia*



National Aeronautics  
and Space Administration

Scientific and Technical  
Information Division

## Summary

A hover test was conducted on a small-scale rotor model for two sets of tapered rotor blades. The baseline rotor-blade set used an NACA 0012 airfoil section, whereas the second rotor-blade set had advanced rotorcraft airfoils RC(4)-10, RC(3)-10, and RC(3)-08 distributed along the radius. The experiment was conducted for a range of thrust coefficients and tip speeds, and the data were compared with the predictions of three analytical methods. The data show the advantage of the advanced airfoils at the higher rotor thrust levels; two of the methods predicted the correct data trends.

## Introduction

The helicopter rotor airfoil is required to operate in a complex rotating aerodynamic environment. In forward flight, the rotational velocity of the rotor blades and the free-stream velocity combine to produce periodic loading and unloading of the rotor blades. When the blade is advancing into the flight direction, the local velocity is high and the blade produces high lift. However, when the blade is retreating from the flight direction, the relative velocity is low; the local velocity may even be reversed with respect to the airfoil on the rotor. Therefore, the retreating blade operates at a lower lift than the advancing blade. This imbalance in lift causes a rolling moment about the rotor hub. In order to balance the lift and "zero" the moments, the advancing blade is usually operated at lower angles of attack than the retreating blade, whereas the retreating blade is operated at angles of attack near the stall limit.

These variations in local blade velocity and angle of attack place several conflicting restrictions on rotor airfoils. (See refs. 1 to 4.) The outboard portion of the advancing blade operates in a low-lift, high-velocity region. Therefore, the airfoil is required to have a high drag-divergence Mach number at low lift to avoid excessive drag. The data in reference 2 suggest that a symmetric or slightly cambered thin airfoil section would have this characteristic. However, the inboard section of the retreating blade requires high-lift capability at low velocity. It is shown in references 2 and 5 that a thick, cambered airfoil would provide this capability. The airfoil also should generate little or no pitching moment at all operating conditions in order to avoid aeroelastic instabilities and high control loads. Even though a symmetric airfoil generates little pitching moment, a cambered airfoil will produce a moment, as the data in reference 5 show.

A compromise among these conflicting requirements for rotor airfoils has resulted in the use of

the NACA 0012 airfoil section on many helicopter rotors (ref. 3). The 12 percent thickness is a compromise between the thin section desired for good compressibility effects and the thick section required for high lift. The symmetric section also generates little pitching moment and is easy to manufacture.

With the recent developments in composite manufacturing technology, it has become possible to build rotor blades with an aerodynamically tailored airfoil distribution along the radius (refs. 6 to 8). This technology allows the rotor designer the freedom to select the optimum airfoil as a function of radial location along the blade, thus increasing the performance of the rotor. The benefits to the vehicle from optimizing the rotor airfoils include a gain in maximum vehicle speed, an increase in gross weight, and more maneuverability (ref. 6). With these types of benefits available, there has been increased interest in designing rotor airfoils.

A series of rotorcraft airfoils (the RC series) was designed by U.S. Army researchers at the NASA Langley Research Center as part of an effort to design an advanced rotor-blade geometry with improved hovering performance and no degradation of forward flight performance. The design philosophy is discussed in reference 8; the rotor is optimized by using combinations of planform, twist, and airfoil distribution to improve rotor performance as predicted by simple computational methods. The hover-prediction method used in this design process was a momentum blade-element analysis based on the theory outlined in reference 9. The forward flight analyses were based on the work in references 10 to 12 and on the rotor flight-simulation code (C81) discussed in reference 13.

The airfoils that were designed for this application were the RC(3)-12, RC(3)-10, and RC(3)-08. In the RC(x)-xx format, the "RC" designates a rotorcraft airfoil, (x) indicates the sequential number, and the "-xx" provides the thickness in percent of chord. These airfoils were tested in two-dimensional wind-tunnel tests, and the results are documented in reference 14 by Bingham and Noonan. These airfoils exhibited high drag-divergence Mach numbers and low pitching moments, but they had average high-lift characteristics. The RC(4)-10, designed and tested by Noonan, proved to have good high-lift capability, but the two-dimensional wind-tunnel test results have not been published at this time.

The RC(3)-12, RC(3)-10, and RC(3)-08 airfoils were used on the wind-tunnel model rotor of reference 15, and the RC(3)-10 and RC(3)-08 airfoils were used during the test of reference 16. The RC(4)-10, RC(3)-10, and RC(3)-08 airfoils were used on the model rotor in reference 17. In these test

programs, performance gains were measured for the rotors with the RC-series airfoils. The gains were seen in terms of increased rotor efficiency in hover and power reductions in forward flight. However, the effect of only the airfoils on rotor performance could not be determined from these tests because the advanced airfoil rotor blades also included changes in planform and twist distribution from the baseline blade.

The purpose of the present investigation was to determine the hover-performance benefits that are gained solely through use of the advanced rotor airfoils. Therefore, a hover study was conducted using rotor systems for which the only difference was airfoil shape. This hover test used a small-scale, four-bladed rotor model with two tapered rotors. The reference rotor used an NACA 0012 airfoil, whereas the second rotor had advanced rotorcraft airfoils RC(4)-10, RC(3)-10, and RC(3)-08 distributed along the blade span. The rotors were identical in planform and twist distribution, and they were tested over a range of thrust coefficients and tip speeds. The experimental data were compared with the hover performance predicted by three analytical methods. One of the methods used a momentum blade-element analysis, whereas the other two methods used a free-wake lifting-surface analysis.

## Symbols

The data in this report were measured in U.S. Customary Units and are referenced to the shaft axis system shown in figure 1.

$C_{d_o}$	rotor profile drag coefficient
$C_Q$	rotor torque coefficient, $M_Z / \rho \pi R^3 (\Omega R)^2$
$C_{Q_o}$	rotor torque coefficient at zero thrust
$C_T$	rotor thrust coefficient, $T / \rho \pi R^2 (\Omega R)^2$
$c$	local blade chord, ft
$c_q$	torque-weighted equivalent blade chord, $\frac{\int_0^1 c(r/R)^3 d(r/R)}{\int_0^1 (\tau/R)^3 d(\tau/R)}$ , ft
$D$	rotor drag force, lbf
FM	rotor figure of merit, $C_T^{3/2} / C_Q \sqrt{2}$
(FM)*	alternate rotor figure of merit, $C_T^{3/2} / (C_Q - C_{Q_o}) \sqrt{2}$

$L$	rotor lift force, lbf
$M_{tip}$	rotor tip Mach number
$M_Z$	rotor torque, ft-lbf
$N_{Re}$	Reynolds number, $\rho V c / \mu$
$R$	rotor radius, ft
$r$	radial distance along blade, ft
$T$	rotor thrust, $(L^2 + D^2 + Y^2)^{1/2}$ , lbf
$V$	local velocity, ft/sec
$V_{tip}$	rotor tip speed, ft/sec
$x, y, z$	Cartesian coordinates
$Y$	rotor side force, lbf
$\mu$	coefficient of viscosity, slugs/ft-sec
$\rho$	atmospheric density of air, slugs/ft <sup>3</sup>
$\sigma_Q$	torque-weighted solidity, $4c_q / \pi R$
$\Omega$	rotor rotational speed, rad/sec

## Abbreviations and acronyms:

HOVER	lifting-surface hover-performance code
LSAF	Lifting-Surface Aerodynamics and Performance Analysis of Rotors in Axial Flight
ROBIN	generic fuselage shell
RTC	rotor test cell
2MRTS	2-meter rotor test system

## Model and Test Description

The test program was conducted in the rotor test cell (RTC) at the Langley 14- by 22-Foot Subsonic Tunnel. The RTC is a high-bay area that is 69 ft high by 42 ft wide by 48 ft long with a steel chain link fence around the walls; it is arranged specifically for the buildup and testing of powered rotor models in hover. Two walls of the RTC have louvers that can be opened to alleviate some of the recirculation of air from the hovering rotor. The ambient dry-bulb temperature, dew point, and pressure are measured by instrumentation located in the RTC. The rotor hub was located 1.74 rotor diameters above the floor of the RTC on a post mount. The model is pictured mounted for testing in the RTC in figure 2.

The model system used for the experiment was the 2-meter rotor test system (2MRTS) with a generic fuselage shell (ROBIN). The ROBIN fuselage shape is detailed in reference 18, and the 2MRTS is documented in reference 19. A brief description of the 2MRTS is repeated here for the convenience of the reader.

The 2MRTS (fig. 2) is a drive system that consists of a 29-hp electric motor, a 90°, two-stage transmission with a 4-to-1 gear reduction ratio, and a four-bladed rotor hub. The motor is water cooled by a chiller system, and the transmission is cooled and lubricated by an oil pump and vacuum system. The motor, transmission, and rotor hub are all suspended on a gimbal that allows the system to pitch and roll; however, both the pitching and rolling motions are damped by mechanical dampers in order to avoid a ground resonance condition. The rotor hub is a four-bladed, fully articulated hub with coincident flap and lag hinges. The lagging motion of the blades is damped by viscous dampers.

The collective and cyclic angles of the rotating blades are controlled through a conventional swash plate mechanism. The swash plate is positioned by three actuators that are remotely controlled at an operator's console. The control of the actuators is accomplished in a feedback-loop control system using a minicomputer to calculate the position of the actuators for the desired rotor-blade pitch angle.

Forces and moments are measured separately on the rotor and fuselage by two six-component, strain gauge balances. Other instrumentation of the system includes three strain gauges on the rotor blades to measure bending moments, potentiometers to measure flapping and lead-lag motion, a digital rotational speed encoder, and thermocouples to monitor critical temperatures in the motor, transmission, and swash plate.

The two sets of rotor blades used in this investigation are described in figure 3. The blade sets differed only by airfoil sections. The baseline set of blades was constructed using NACA 0012 airfoils. The second set of blades had advanced airfoils specifically designed for the rotating environment (RC(4)-10, RC(3)-10, and RC(3)-08) distributed along the blade radius, as shown in figure 3. Smooth transitions were accomplished between airfoil sections over 5 percent of the blade radius. The three airfoil sections, together with the NACA 0012 section, are shown in figure 4; the coordinates for the advanced airfoils are given in tables I, II, and III. Both sets of rotor blades had a tapered planform (with the 3-to-1 taper ratio initiating at 75 percent of the 32.5-in. radius) and a -13° linear twist distribution. The thrust-weighted solidity of the rotor was 0.0977. The rotor blades

were constructed using a graphite-epoxy D-spar with tungsten leading-edge weights. The baseline blades had a foam trailing edge, whereas the advanced airfoil blades had a balsa trailing edge. Both sets of blades were very stiff, as there was no attempt to match the aeroelastic characteristics of full-scale rotor blades.

The test procedure was as follows: the rotor rotational speed was established and maintained, a collective blade angle was input, and the shaft angle was set to zero. The flapping of the rotor blades was monitored and was maintained within a tenth of a degree of zero during the test. When the model was at a test point condition, a data point was taken. After the data had been collected, the collective angle was increased and the procedure was repeated. The upper limit of the thrust sweep was determined by motor power and temperature; i.e., when the drive motor exceeded critical temperatures, the thrust sweep was terminated. Thrust sweeps were made at rotational speeds from 2000 to 2500 rpm for a range of thrust coefficients  $C_T$  from 0 to approximately 0.010 for each set of rotor blades.

The data were acquired through a static data acquisition system that sampled the data. Four hundred data measurements were acquired in 8 sec for each data point presented. Each thrust sweep was repeated three times in order that some measure of the data accuracy and scatter could be determined. One condition was tested on 2 different days in order to ensure that daily variances in temperature, humidity, and pressure were being properly corrected. The ambient winds in the RTC were measured daily, and data were acquired only when the wind conditions were in the range from 0 to 1 knot. The precision of the data measurements is estimated from the repeatability tests to be  $\pm 2.5 \times 10^{-4}$  in thrust coefficient  $C_T$ ,  $\pm 0.01$  in rotor figure of merit FM, and  $\pm 3.0 \times 10^{-5}$  in torque coefficient  $C_Q$ .

## Description of Analytical Methods

The selection of the hover analytical methods used for this investigation was based on the experience with hover-performance codes in reference 20 and the desire to investigate the capabilities of the relatively new lifting-surface free-wake hover codes. It should be recognized that there are many different prediction methods under development; the codes used in this effort are only a representative sample. It was found in reference 20 that a simple momentum blade-element analysis was able to predict hover data trends. It was also found in that study that the simple free-wake analysis of reference 21 was unable to converge on a solution, whereas the prescribed-wake lifting-line analysis of reference 22 predicted

the wrong trends for the hover performance of tapered rotor-blade configurations. Therefore, it was decided to use two sophisticated lifting-surface free-wake analyses as well as the simple momentum blade-element theory for this investigation.

The momentum blade-element analysis used for this investigation is a code based on the equations developed in reference 9. The rotor disk is assumed to be an infinitely thin actuator disk that allows no velocity discontinuities across the disk. The induced vertical velocity through the rotor disk is found by equating the change in the momentum of the air to the thrust of the rotor. Then, the rotor blade is considered to be a combination of individual airfoil segments, and the forces on each section are calculated. The airfoil section properties are obtained from tables of two-dimensional airfoil data. The total rotor forces are determined by integrating the segment forces over the rotor blade.

The second analytical method used in this investigation was the lifting-surface hover-performance code (HOVER). The method is documented in reference 23. The rotor blades are modeled using a vortex-lattice panel distribution, whereas the wake is represented by discrete vortex segments. The rotor wake geometry is determined through two sets of iterations. The first iteration set consists of establishing a wake geometry from a set of prescribed-wake equations and matching the circulation solution of the rotor blades. In the second iteration set, the rotor wake is allowed to distort as a free wake from the generalized wake solution in response to the induced velocities from the rotor blades and from self-induced velocities in the wake itself. After a wake geometry has been determined, HOVER calculates the circulation induced by the wake at the rotor-blade surface through use of the Biot-Savart Law. Once the circulation is known, the lift can be calculated from the Kutta-Joukowski Law. The drag is calculated by combining the induced drag with the airfoil profile drag from two-dimensional airfoil data. The rotor torque is calculated from the integrated rotor-blade drag. There is no model for stall or separation in HOVER. Compressibility effects on lift are calculated using a Prandtl-Glauert correction, whereas the effects on drag are assumed to be contained in the two-dimensional airfoil data tables.

The third analytical method used in this investigation was the Lifting-Surface Aerodynamics and Performance Analysis of Rotors in Axial Flight (LSAF) which is discussed in reference 24. The rotor blades and wake were represented as vortex boxes, or lattices. The version of LSAF that was used for this study incorporated a velocity-coupled wake model into the program in addition to the prescribed-wake

model discussed in reference 25. The calculations for the rotor performance are similar to those used in HOVER; i.e., the lift is calculated using the circulation distribution, and the drag and torque calculations rely on two-dimensional airfoil data.

## Presentation of Results

The experimental data are presented in tabular and graphical format. The values of thrust coefficient  $C_T$ , torque coefficient  $C_Q$ , and figure of merit FM for the baseline and advanced airfoil rotor blades can be found in tables IV and V, respectively. The analytical comparisons to the experimental data are shown graphically. The presentations are made using the following figures:

	Figure
Basic aerodynamic characteristics of rotors for several $M_{tip}$ values . . . . .	5
Comparison of aerodynamic characteristics of baseline and advanced rotors . . . . .	6
Power required to hover for baseline and advanced rotors at $M_{tip} = 0.639$ . . . . .	7
Comparison of an alternate figure of merit for the baseline and advanced airfoil rotors at $M_{tip} = 0.639$ . . . . .	8
Comparison of prediction methods with experimental data at $M_{tip} = 0.639$ . . . . .	9
Comparison of three analytical methods at $M_{tip} = 0.639$ . . . . .	10
Effect of two-dimensional airfoil data tables on analytical results for baseline rotor at $M_{tip} = 0.639$ . . . . .	11
Comparison of analytical predictions for several values of $M_{tip}$ . . . . .	12
Effect of user input for radial position $r/R$ of maximum circulation on performance calculations by HOVER at $M_{tip} = 0.639$ . . . . .	13

## Results and Discussion

### Experimental Results

The results of the experiment are shown in figure 5 as plots of figure of merit FM versus thrust coefficient  $C_T$ . Figure of merit is an efficiency term that expresses the ratio of the ideal power required for hover to the actual power required for hover.

The data for the baseline rotor are shown in figure 5(a) for several tip Mach numbers. The data show very similar trends below  $C_T = 0.007$ ; however, at the higher thrust coefficients, there is a decreasing efficiency trend with increasing tip Mach number. This trend can be attributed to the decreased maximum lift coefficient and increase in drag of the

baseline NACA 0012 airfoil that is associated with an increase in Mach number.

The performance of the advanced airfoil rotor is shown in figure 5(b) for the same three tip Mach numbers. The effect of Mach number on the advanced airfoil rotor is not the same as that observed for the 0012 airfoil rotor. This difference in behavior may be attributed to the different Mach number characteristics of the advanced airfoil sections. From the two-dimensional airfoil data in references 14 and 26, it is known that the outboard advanced airfoils experience an increase in maximum normal-force coefficient with increased Mach number in the range of Mach numbers tested, whereas the maximum lift of the 0012 airfoil decreases in this Mach number range.

The experimental data for the baseline 0012 rotor and the advanced airfoil rotor are compared in figure 6. As was evident in the earlier figures, the advanced airfoil rotor performs more efficiently than the baseline 0012 airfoil rotor at the higher thrust coefficients. Torque coefficient  $C_Q$  is plotted against thrust coefficient  $C_T$  to provide an indication of the power required by the rotor for the highest and lowest tip Mach numbers.

The rotor efficiency term, i.e., the figure of merit FM, has been traditionally defined (ref. 9) for hovering rotors as

$$FM = C_T^{3/2} / C_Q \sqrt{2} \quad (1)$$

This expression relates the lowest possible power required for hover with an ideal rotor to the actual power required for hover. This definition assumes that the ideal rotor has zero power, or torque, required as a result of the effects of profile drag. Since the operating rotor actually does experience the effects of profile drag, to compare only the torque produced by the induced drag requires that the torque generated by the rotor profile drag be removed from the data. An approximation of the torque due to the profile drag  $C_{Q_o}$  is obtained by plotting  $C_Q$  against  $C_T^{3/2}$  and extrapolating the data to the zero thrust condition (ref. 27). The result is only an approximation of the torque due to profile drag effects because the rotor is twisted; therefore, even at the zero thrust condition, a small portion of the measured torque is due to induced effects. However, it is the best approximation to the true profile torque effects that can be made from these data. When the torque due to profile drag is removed, an expression for an alternate figure of merit that compares only the induced power effects is obtained:

$$(FM)^* = C_T^{3/2} / (C_Q - C_{Q_o}) \sqrt{2} \quad (2)$$

Figure 7 is a plot of  $C_Q$  against  $C_T^{3/2}$  for the baseline and advanced airfoil rotors at a tip Mach number of 0.639. The  $C_{Q_o}$  for the baseline 0012 rotor was found from the intercept of a second-order least-squares curve fit to be 0.00012, and the  $C_{Q_o}$  for the advanced airfoil was 0.00013. In figure 8, the alternate figure of merit (FM)\* is plotted as a function of  $C_T$  for the baseline and advanced airfoil rotors at the tip Mach number of 0.639. The data are not plotted for the lower thrust coefficients because the  $C_Q$  measurement became approximately equal to  $C_{Q_o}$ , and (FM)\* became meaningless. When compared using this alternate figure of merit, the advanced airfoil rotor was found to have a higher (FM)\* than the baseline 0012 rotor over this  $C_T$  range. This effect indicated that the advanced airfoil rotor had greater efficiency in producing lift than the baseline rotor, although the advantage of the advanced airfoil rotor in terms of overall efficiency (induced and profile drag effects) occurred at the higher thrust coefficients. (See fig. 6.) From this analysis, it can be concluded that if the profile drag of the advanced airfoil rotor could be reduced, the advanced airfoil rotor would have an improvement in efficiency (FM) over the baseline rotor for the entire thrust range.

### Analytical Results

The prediction of performance by analytical methods can be used for several different purposes. For example, a rotor designer needs an analysis that will predict the correct trends in performance for a systematic parametric study. Another use for the analyses is to predict the level of performance that would be expected for a given rotor. Figure 9 shows the ability of several analytical methods to predict performance trends, whereas figure 10 compares the ability of the analytical methods to predict performance levels. In all cases, a tension spline was applied to the analytical predictions to produce the curves shown in the figures, and airfoil data obtained at full-scale Reynolds numbers were used to make the predictions.

It can be seen in figure 9 that both the momentum analysis and the HOVER analysis predicted an improvement in performance for the advanced airfoil rotor. However, both methods predicted that the improvement occurred at a higher thrust coefficient than was measured in the experiment, as expected because of the use of airfoil data obtained at full-scale Reynolds numbers. The LSAF method prediction, which is shown in figure 9(c), exhibited signs of numerical instability at thrust coefficients greater than 0.0102.

In figure 10 it is shown that the HOVER analysis predicts the figure of merit levels of the experimental rotor model more accurately than the other two methods for both the baseline 0012 rotor and the advanced airfoil rotor. In order to investigate the effect of using the full-scale airfoil data, a sensitivity study of the effects of the two-dimensional airfoil tables was conducted using the momentum analysis and HOVER methods.

The two-dimensional data for the NACA 0012 airfoil were obtained from tests in the Langley 6-by 28-Inch Transonic Tunnel for two Reynolds number ranges (ref. 26), one representing model-scale and the other full-scale helicopter Reynolds numbers. The lower Reynolds number range was  $0.7 \times 10^6$  to  $1.5 \times 10^6$ , and the higher Reynolds number range was  $3.0 \times 10^6$  to  $6.6 \times 10^6$ . The advanced airfoil two-dimensional data were available only for representative full-scale Reynolds numbers. The experimental rotor operated at a tip Reynolds number of  $0.39 \times 10^6$  and an inboard maximum Reynolds number at 75-percent radius of  $0.89 \times 10^6$ . In figure 11, the performance predicted by the momentum analysis and HOVER methods is shown for different two-dimensional airfoil tables for the baseline 0012 rotor at a tip Mach number of 0.639. Calculations are shown for both the higher and lower Reynolds number airfoil data, as well as calculations performed using a modified high Reynolds number data table. The modification to the data table consisted of increasing the drag coefficient in the table by the difference between the  $C_{d_o}$  in the data table and the  $C_{d_o}$  determined from the data of this test (where  $C_{d_o} = 8C_{Q_o}/\sigma Q$ ). This modification was selected based on reference 27 where it was suggested that the increment in performance between the model-scale and full-scale values was due to the difference in rotor profile drag.

As was expected, the calculations by both methods indicated that the use of the lower Reynolds number data table decreased the predicted performance of the rotor. In the case of the momentum analysis, the predicted FM was closer to the experimental data, whereas for HOVER the lower Reynolds number predictions were farther from the experimental data than the full-scale Reynolds number predictions. The HOVER program appears to be able to predict the correct model-rotor performance level only when using the airfoil tables obtained at full-scale Reynolds numbers. This result is fortunate because the full-scale airfoil data are generally the only data available to the user for advanced rotorcraft airfoil sections.

Figure 12 shows the ability of the analyses to predict the variation in rotor performance with tip

Mach number. Both the momentum analysis and the HOVER methods predicted the trend that was measured for the baseline 0012 rotor. However, the momentum analysis predicted a change in rotor performance for the advanced airfoil rotor that was not present in the experimental data as a result of changing the tip Mach number. HOVER also predicted some effects of changing the tip Mach number for the advanced rotor, especially at a thrust coefficient of 0.011.

The values calculated by the HOVER and LSAF performance codes were affected greatly by user input. During this investigation, it was found that the LSAF calculations were sensitive to user inputs such as number of wake iterations, increment in thrust level, starting values of thrust and control angles, and wake azimuth increments. The program was not able to converge on a solution for most of the input variations that were attempted. The tapered planform of the rotor blades may have been a factor in the numerical instability of the LSAF code; the blade-load distribution due to the taper may have triggered a computational instability between the wake geometry and the circulation solution.

This type of problem was also apparent in the HOVER program. In the HOVER input, the user was allowed to specify how the radial position of maximum circulation is determined through an input parameter. The effect that this decision may have on the values calculated by HOVER is shown in figure 13. HOVER was executed for three cases. In the first case, the position of maximum circulation was held at a constant radial position throughout the prescribed-wake iterations of HOVER, but the program was free to move the position when it started the free-wake geometry perturbations. For the second case, the position of maximum circulation was held at a constant radial position of 75 percent throughout the entire prescribed-wake and free-wake geometry calculations. The third case allowed HOVER to have the freedom to determine the position of maximum circulation during each wake geometry iteration. As can be seen in figure 13, for both the baseline 0012 and the advanced airfoil rotors at a tip Mach number of 0.639, the calculations were closest to the experimental data when the radial position was held at a constant value throughout the prescribed-wake calculations and was then allowed to change position during the free-wake iterations. The question remains as to how the constant radial value should be obtained; in order to be consistent, some criteria should be imposed for determining this value. For this investigation, the radial position of maximum circulation that was calculated in the momentum blade-element analysis was used as the

input into HOVER. This combination of the momentum analysis and HOVER methods provided good agreement with these experimental data. Further studies are required to determine whether this combination will prove to be a consistently reliable method.

## Summary of Results

A hover test was conducted on a small-scale rotor model for two sets of tapered rotor blades. The baseline rotor-blade set used an NACA 0012 airfoil section, whereas the second rotor-blade set used three advanced rotorcraft airfoil sections distributed along the radius. Both blade sets had identical planform and twist distributions. The experiment was conducted for a range of thrust coefficients and tip speeds, and the data were compared with the predictions of three analytical methods. The methods used in this investigation were a simple momentum blade-element analysis and two free-wake lifting-surface hover-performance analyses (HOVER and LSAF). The results of the investigation and the comparison are summarized as follows:

1. The experimental data show that for the three speeds investigated at the higher thrust levels (above a thrust coefficient  $C_T$  of 0.007), the advanced airfoil rotor had better hover performance than that of the baseline NACA 0012 rotor.

2. The baseline NACA 0012 rotor experienced some detrimental Mach number effects for  $C_T$  above 0.007 at the higher tip Mach numbers. The advanced airfoil rotor data did not show any effect of the tip Mach number variation.

3. Of the three analytical methods used for this study, the lifting-surface analysis HOVER and the momentum analysis predicted the greater efficiency of the advanced airfoil rotor at the higher thrust coefficients.

4. The predictions of both lifting-surface analyses used in this study were very sensitive to the user inputs. It was found that using the output of the momentum analysis as a guide for the input into HOVER resulted in a prediction that was in general agreement with the experimental data.

NASA Langley Research Center  
Hampton, VA 23665-5225  
August 5, 1988

## References

- Stepniewski, W. Z.; and Keys, C. N.: *Rotary-Wing Aerodynamics*. Dover Publ., Inc., 1984.  
Stepniewski, W. Z.: *Volume I: Basic Theories of Rotor Aerodynamics (With Application to Helicopters)*.
- Keys, C. N.: *Volume II: Performance Prediction of Helicopters*.
- Davenport, Franklyn J.; and Front, John V.: Airfoil Sections for Helicopter Rotors—A Reconsideration. *Proceedings of the Twenty-Second Annual National Forum*, American Helicopter Soc., Inc., May 1966, pp. 29-44.
- Johnson, Wayne: *Helicopter Theory*. Princeton Univ. Press, c.1980.
- Dadone, Leo: Rotor Airfoil Optimization: An Understanding of the Physical Limits. Preprint No. 78-4, *34th Annual National Forum*, American Helicopter Soc., Inc., May 1978.
- Abbott, Ira H.; and Von Doenhoff, Albert E.: *Theory of Wing Sections*. Dover Publ., Inc., c.1959.
- Thibert, Jean-Jacques; and Gallot, Jacques: Advanced Research on Helicopter Blade Airfoils. *Vertica*, vol. 5, no. 3, 1981, pp. 279-300.
- McVeigh, Michael A.; and McHugh, Francis J.: Influence of Tip Shape, Chord, Blade Number, and Airfoil on Advanced Rotor Performance. *J. American Helicopter Soc.*, vol. 29, no. 4, Oct. 1984, pp. 55-62.
- Bingham, Gene J.: The Aerodynamic Influences of Rotor Blade Airfoils, Twist, Taper and Solidity on Hover and Forward Flight Performance. *Proceedings of the 37th Annual Forum*, American Helicopter Soc., May 1981, pp. 37-50.
- Gessow, Alfred; and Myers, Garry C., Jr.: *Aerodynamics of the Helicopter*. Macmillan Co., c.1952. (Republished 1985 by College Park Press.)
- Gessow, Alfred: *Equations and Procedures for Numerically Calculating the Aerodynamic Characteristics of Lifting Rotors*. NACA TN 3747, 1956.
- Gessow, Alfred; and Crim, Almer D.: *A Method for Studying the Transient Blade-Flapping Behavior of Lifting Rotors at Extreme Operating Conditions*. NACA TN 3366, 1955.
- Gessow, Alfred; and Tapscott, Robert J.: *Tables and Charts for Estimating Stall Effects on Lifting-Rotor Characteristics*. NASA TN D-243, 1960.
- Van Gaasbeek, J. R.: *Rotorcraft Flight Simulation, Computer Program C81. Volume II—User's Manual*. USARTL-TR-77-54B, U.S. Army, Oct. 1979. (Available from DTIC as AD A079 632.)
- Bingham, Gene J.; and Noonan, Kevin W.: *Two-Dimensional Aerodynamic Characteristics of Three Rotorcraft Airfoils at Mach Numbers From 0.95 to 0.90*. NASA TP-2000, AVRADCOM TR 82-B-2, 1982.
- Berry, John D.: *Performance Testing of a Main Rotor System for a Utility Helicopter at 1/4 Scale*. NASA TM-83274, AVRADCOM TR 82-B-3, 1982.
- Kelley, H. L.; and Wilson, J. C.: Aerodynamic Performance of a 27-Percent-Scale AH-64 Wind-Tunnel Model With Baseline/Advanced Rotor Blades. *Proceedings of the 41st Annual Forum*, American Helicopter Soc., May 1985, pp. 491-499.
- Yeager, William T., Jr.; Mantay, Wayne R.; Wilbur, Matthew L.; Cramer, Robert G., Jr.; and Singleton, Jeffrey D.: *Wind-Tunnel Evaluation of an Advanced Main-Rotor Blade Design for a Utility-Class Helicopter*. NASA TM-89129, AVSCOM TM 87-B-8, 1987.

18. Freeman, Carl E.; and Mineck, Raymond E.: *Fuselage Surface Pressure Measurements of a Helicopter Wind-Tunnel Model With a 9.15-Meter Diameter Single Rotor*. NASA TM-80051, 1979.
19. Phelps, Arthur E., III; and Berry, John D.: *Description of the U.S. Army Small-Scale 2-Meter Rotor Test System*. NASA TM-87762, AVSCOM TM 86-B-4, 1987.
20. Phelps, Arthur E., III; and Althoff, Susan L.: *Effects of Planform Geometry on Hover Performance of a 2-Meter-Diameter Model of a Four-Bladed Rotor*. NASA TM-87607, AVSCOM TR 85-B-6, 1986.
21. Miller, R. H.: *Simplified Free Wake Analyses for Rotors*. ASRL TR 194-3, Dep. of Aeronautics & Astronautics, Massachusetts Inst. of Technology, Aug. 1981.
22. Landgrebe, Anton J.: *An Analytical and Experimental Investigation of Helicopter Rotor Hover Performance and Wake Geometry Characteristics*. USAAMRDL Tech. Rep. 71-24, U.S. Army, June 1971. (Available from DTIC as AD 728 835.)
23. Summa, J. Michael: *Advanced Rotor Analysis Methods for the Aerodynamics of Vortex/Blade Interactions in Hover*. *Eighth European Rotorcraft and Powered Lift Aircraft Forum* (Aix-en-Provence, France), Aug.-Sept. 1982, Paper No. 2.8.
24. Kocurek, J. David; and Berkowitz, Lenard F.: *Velocity Coupling—A New Concept for Hover and Axial Flow Wake Analysis and Design*. *Prediction of Aerodynamic Loads on Rotorcraft*, AGARD-CPP-334, Apr. 1982, pp. 8-1—8-13.
25. Kocurek, J. David; and Tangler, James L.: *A Prescribed Wake Lifting Surface Hover Performance Analysis*. *J. American Helicopter Soc.*, vol. 22, no. 1, Jan. 1977, pp. 24-35.
26. Noonan, Kevin W.; and Bingham, Gene J.: *Aerodynamic Characteristics of Three Helicopter Rotor Airfoil Sections at Reynolds Numbers From Model Scale to Full Scale at Mach Numbers From 0.95 to 0.90*. NASA TP-1701, AVRADCOM TR 80-B-5, 1980.
27. Keys, Charles N.; McVeigh, Michael A.; Dadone, Leo; and McHugh, Francis J.: *Considerations in the Estimation of Full-Scale Rotor Performance From Model Rotor Test Data*. *Proceedings of the 39th Annual Forum of the American Helicopter Society*, May 1983, pp. 34-43.

Table I. Airfoil Coordinates for RC(4)-10

[Stations and ordinates given in fraction of airfoil chord]

Station	Lower surface	Station	Upper surface
1.000000	0.000203	0.000000	-0.005726
.975148	-.003160	.002864	.004313
.950227	-.005728	.009072	.013175
.925298	-.008079	.023543	.025980
.900374	-.010312	.047036	.038875
.875421	-.012443	.073686	.047953
.850386	-.014420	.100188	.053673
.825282	-.016215	.126143	.057324
.800114	-.017818	.151842	.059790
.774866	-.019273	.177227	.061579
.749797	-.020610	.202556	.062995
.724840	-.021873	.227760	.064163
.699792	-.023108	.252956	.065143
.674849	-.024327	.303145	.066614
.649997	-.025542	.353142	.067381
.625136	-.026750	.378140	.067422
.600297	-.027933	.403297	.067163
.575437	-.029062	.428390	.066543
.550567	-.030090	.453678	.065499
.525714	-.030972	.478891	.064013
.500894	-.031659	.503763	.062129
.476002	-.032163	.528707	.059876
.451451	-.032474	.553618	.057324
.426974	-.032600	.578512	.054510
.402303	-.032553	.603417	.051447
.377696	-.032369	.628341	.048144
.352929	-.032090	.653244	.044621
.303398	-.031393	.678157	.040912
.254059	-.030703	.702978	.037093
.229490	-.030430	.727694	.033251
.204930	-.030257	.752502	.029451
.180495	-.030276	.777197	.025808
.156116	-.030611	.801713	.022378
.132051	-.031269	.826309	.019139
.108242	-.032011	.850970	.016086
.084979	-.032337	.875699	.013211
.061865	-.031576	.900509	.010514
.035595	-.028199	.925350	.008012
.025184	-.025664	.950185	.005722
.016462	-.022703	.975028	.003652
.014350	-.021823	1.000000	.001785
.004687	-.015907		

Table II. Airfoil Coordinates for RC(3)-10

[Stations and ordinates given in fraction of airfoil chord]

Station	Lower surface	Station	Upper surface
1.00000	-0.00020	0.00000	0.00000
.96828	-.00633	.00310	.00906
.93631	-.01171	.01090	.01700
.90409	-.01594	.02403	.02462
.87082	-.01959	.04214	.03193
.83623	-.02272	.06347	.03854
.80002	-.02536	.08724	.04435
.76185	-.02758	.11305	.04944
.72232	-.02939	.14075	.05376
.68276	-.03079	.17023	.05748
.64378	-.03184	.20137	.06051
.60547	-.03260	.23402	.06292
.56746	-.03313	.26807	.06474
.52949	-.03346	.30343	.06596
.49148	-.03360	.33995	.06661
.45336	-.03357	.37733	.06672
.41524	-.03337	.41524	.06627
.37733	-.03301	.45336	.06528
.33995	-.03249	.49148	.06376
.30343	-.03184	.52949	.06170
.26807	-.03107	.56746	.05909
.23402	-.03020	.60547	.05593
.20137	-.02923	.64378	.05220
.17023	-.02817	.68276	.04787
.14075	-.02696	.72232	.04296
.11305	-.02561	.76185	.03758
.08724	-.02400	.80002	.03200
.06347	-.02203	.83623	.02644
.04214	-.01950	.87082	.02096
.02403	-.01619	.90409	.01564
.01090	-.01230	.93631	.01052
.00310	-.00765	.96828	.00600
		1.00000	.00180

Table III. Airfoil Coordinates for RC(3)-08

[Stations and ordinates given in fraction of airfoil chord]

Station	Lower surface
1.00000	-0.00050
.96782	-.00513
.93543	-.00942
.90280	-.01293
.86927	-.01599
.83457	-.01867
.79842	-.02099
.76057	-.02300
.72150	-.02469
.68238	-.02605
.64367	-.02713
.60553	-.02796
.56766	-.02858
.52983	-.02902
.49199	-.02929
.45404	-.02939
.41612	-.02934
.37840	-.02913
.34121	-.02877
.30484	-.02853
.26959	-.02791
.23560	-.02693
.20298	-.02609
.17186	-.02513
.14239	-.02403
.11471	-.02278
.08889	-.02129
.06508	-.01951
.04369	-.01729
.02534	-.01445
.01170	-.01096
.00314	-.00656

Station	Upper surface
0.00000	0.00000
.00314	.00671
.01170	.01312
.02534	.01900
.04369	.02455
.06508	.02952
.08889	.03389
.11471	.03770
.14239	.04096
.17186	.04376
.20298	.04606
.23560	.04789
.26959	.04928
.30484	.05023
.34121	.05075
.37840	.05087
.41612	.05057
.45404	.04986
.49199	.04876
.52983	.04725
.56766	.04533
.60553	.04300
.64367	.04024
.68238	.03704
.72150	.03342
.76057	.02944
.79842	.02528
.83457	.02107
.86927	.01686
.90280	.01271
.93543	.00864
.96782	.00490
1.00000	.00130

Table IV. Experimental Data for Baseline 0012 Rotor

$V_{tip}$ , fps	$C_T$	FM	$C_Q$	$V_{tip}$ , fps	$C_T$	FM	$C_Q$
567	0.00072	0.104	0.000128	638	0.00067	0.094	0.000130
	.00074	.114	.000125		.00071	.100	.000132
	.00123	.211	.000143		.00079	.117	.000133
	.00123	.208	.000147		.00115	.187	.000147
	.00124	.212	.000146		.00128	.212	.000153
	.00176	.301	.000174		.00131	.218	.000153
	.00178	.313	.000169		.00175	.297	.000174
	.00188	.329	.000175		.00177	.298	.000177
	.00238	.405	.000202		.00191	.325	.000182
	.00242	.411	.000205		.00243	.409	.000207
	.00247	.414	.000210		.00245	.406	.000211
	.00313	.496	.000249		.00249	.408	.000215
	.00320	.502	.000254		.00320	.499	.000256
	.00320	.491	.000260		.00325	.495	.000265
	.00411	.577	.000322		.00327	.509	.000259
	.00412	.582	.000321		.00403	.563	.000321
	.00416	.572	.000331		.00420	.578	.000333
	.00505	.632	.000402		.00426	.579	.000340
	.00510	.626	.000411		.00457	.606	.000359
	.00524	.636	.000422		.00500	.620	.000403
	.00597	.676	.000482		.00510	.637	.000404
	.00604	.668	.000496		.00515	.640	.000408
	.00606	.671	.000497		.00544	.634	.000447
	.00674	.686	.000570		.00545	.646	.000440
	.00677	.677	.000582		.00598	.675	.000484
	.00679	.683	.000579		.00599	.661	.000495
	.00790	.682	.000728		.00615	.660	.000516
	.00807	.687	.000746		.00639	.669	.000539
	.00814	.684	.000758		.00640	.674	.000536
	.00859	.659	.000853		.00679	.675	.000586
	.00876	.666	.000870		.00683	.675	.000591
	.00879	.667	.000873		.00686	.686	.000585
	.00946	.620	.001048		.00725	.673	.000648
	.00976	.635	.001073		.00731	.673	.000656
	.00980	.607	.001128		.00779	.672	.000723

Table IV. Concluded

$V_{tip}$ , fps	$C_T$	FM	$C_Q$
638	0.00785	0.675	0.000727
	.00789	.659	.000751
	.00822	.664	.000793
	.00838	.664	.000816
	.00872	.642	.000896
	.00873	.648	.000890
	.00905	.620	.000980
	.00917	.622	.000998
	709	.00074	.110
.00074		.111	.000128
.00125		.210	.000148
.00130		.221	.000149
.00133		.226	.000152
.00185		.324	.000173
.00185		.325	.000173
.00197		.337	.000184
.00247		.415	.000209
.00251		.432	.000206
.00329		.510	.000261
.00331		.512	.000263
.00336		.517	.000267
.00413		.585	.000320
.00416		.583	.000325
.00431		.598	.000335
.00456		.614	.000355

$V_{tip}$ , fps	$C_T$	FM	$C_Q$
709	0.00465	0.609	0.000368
	.00465	.609	.000368
	.00491	.615	.000395
	.00499	.629	.000396
	.00521	.646	.000412
	.00541	.636	.000442
	.00542	.653	.000431
	.00554	.656	.000444
	.00601	.657	.000502
	.00604	.662	.000501
	.00607	.678	.000493
	.00641	.673	.000539
	.00649	.686	.000538
	.00657	.673	.000559
	.00694	.674	.000606
	.00695	.680	.000603
	.00701	.695	.000597
	.00733	.670	.000662
	.00750	.683	.000671
	.00755	.672	.000690
.00782	.657	.000743	
.00791	.674	.000738	
.00804	.661	.000771	
.00816	.639	.000814	
.00820	.650	.000806	

Table V. Experimental Data for Advanced Airfoil Rotor

$V_{tip}$ , fps	$C_T$	FM	$C_Q$	$V_{tip}$ , fps	$C_T$	FM	$C_Q$	
567	0.00183	0.298	0.000185	567	0.00892	0.690	0.000863	
	.00184	.304	.000184		.00925	.697	.000902	
	.00186	.305	.000185		.00954	.678	.000972	
	.00235	.379	.000213		.00961	.678	.000982	
	.00239	.386	.000214		.00968	.684	.000983	
	.00248	.404	.000215		.00986	.681	.001015	
	.00310	.481	.000254		.00988	.667	.001039	
	.00321	.491	.000262		.01019	.657	.001105	
	.00324	.501	.000260		.01024	.654	.001119	
	.00380	.542	.000306		.01042	.661	.001137	
	.00385	.548	.000309		.01074	.638	.001233	
	.00396	.565	.000312		.01084	.650	.001226	
	.00484	.616	.000386		.01085	.647	.001234	
	.00493	.628	.000389		638	0.00164	0.261	0.000179
	.00499	.629	.000396			.00170	.275	.000180
	.00528	.642	.000422			.00171	.281	.000178
	.00543	.655	.000431	.00233		.378	.000211	
	.00561	.657	.000451	.00240		.394	.000210	
	.00562	.644	.000462	.00240		.391	.000213	
	.00584	.681	.000463	.00310		.475	.000257	
	.00642	.688	.000528	.00317		.488	.000259	
	.00643	.690	.000528	.00321		.505	.000254	
	.00669	.687	.000562	.00374		.539	.000300	
	.00675	.690	.000567	.00381		.550	.000302	
	.00678	.692	.000569	.00388		.562	.000304	
	.00705	.695	.000602	.00462		.608	.000365	
	.00715	.693	.000616	.00465		.612	.000366	
	.00763	.683	.000689	.00471		.615	.000371	
	.00768	.698	.000681	.00582		.660	.000475	
	.00770	.699	.000682	.00590	.673	.000475		
	.00814	.698	.000743	.00591	.662	.000485		
	.00830	.704	.000758	.00668	.684	.000564		
.00849	.690	.000801	.00674	.689	.000567			
.00863	.697	.000813	.00682	.697	.000571			
.00888	.711	.000832	.00765	.706	.000669			

Table V. Concluded

$V_{tip}$ , fps	$C_T$	FM	$C_Q$	
638	0.00768	0.707	0.000672	
	.00770	.705	.000676	
	.00855	.698	.000800	
	.00858	.692	.000811	
	.00872	.705	.000816	
	.00957	.678	.000976	
	.00958	.686	.000967	
	.00963	.682	.000978	
	.01036	.658	.001132	
	.01036	.655	.001138	
	709	0.00114	0.176	0.000155
		.00169	.274	.000180
.00170		.276	.000178	
.00174		.293	.000175	
.00236		.395	.000205	
.00244		.411	.000207	
.00254		.438	.000206	
.00307		.470	.000255	
.00312		.496	.000249	
.00320		.503	.000254	
.00384		.547	.000308	
.00385		.561	.000301	
.00386		.547	.000310	
.00435		.582	.000348	
.00446		.608	.000345	
.00478		.628	.000371	

$V_{tip}$ , fps	$C_T$	FM	$C_Q$
709	0.00479	0.617	0.000380
	.00481	.619	.000381
	.00518	.647	.000407
	.00531	.648	.000422
	.00578	.672	.000463
	.00579	.670	.000464
	.00582	.656	.000478
	.00629	.686	.000513
	.00629	.682	.000517
	.00682	.696	.000572
	.00682	.696	.000572
	.00682	.681	.000585
	.00731	.694	.000636
	.00737	.696	.000642
	.00768	.695	.000685
	.00782	.708	.000691
	.00818	.702	.000744
	.00825	.705	.000751
	.00867	.699	.000817
	.00869	.697	.000820
	.00871	.700	.000820
	.00906	.697	.000875
	.00919	.686	.000908
	.00919	.685	.000908
.00960	.675	.000985	
.00967	.674	.000995	

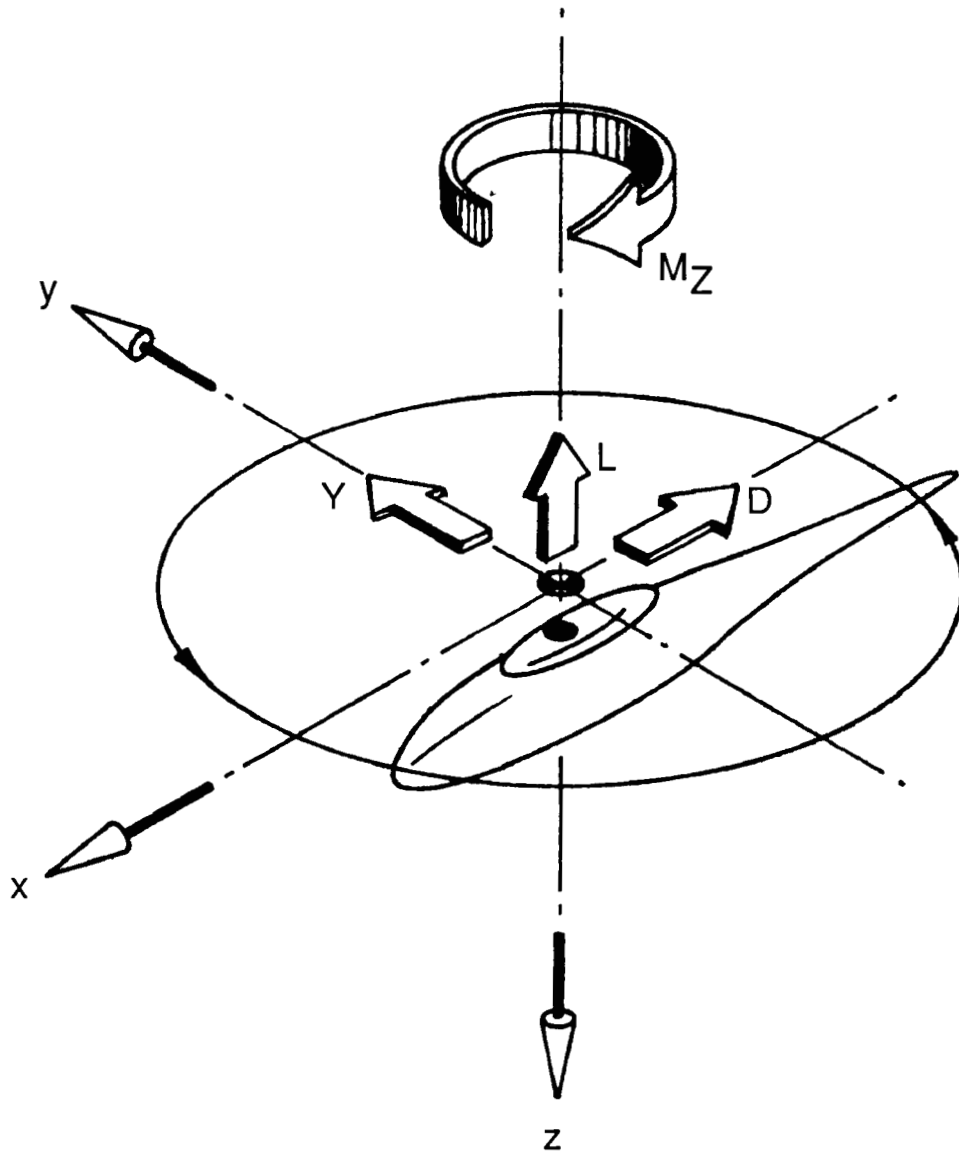
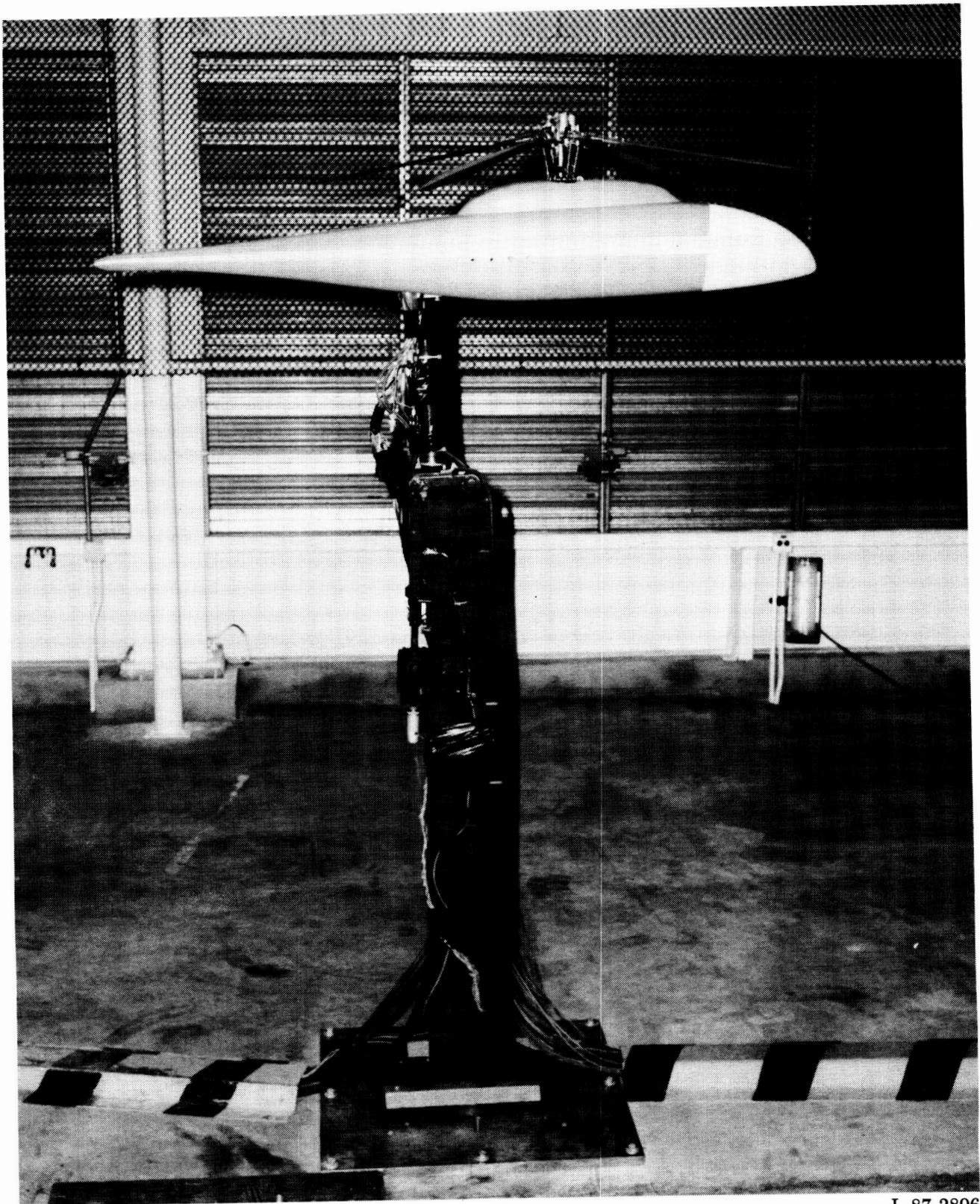


Figure 1. Axis system used for presentation of data. Arrows denote positive directions of forces, moments, and axes.

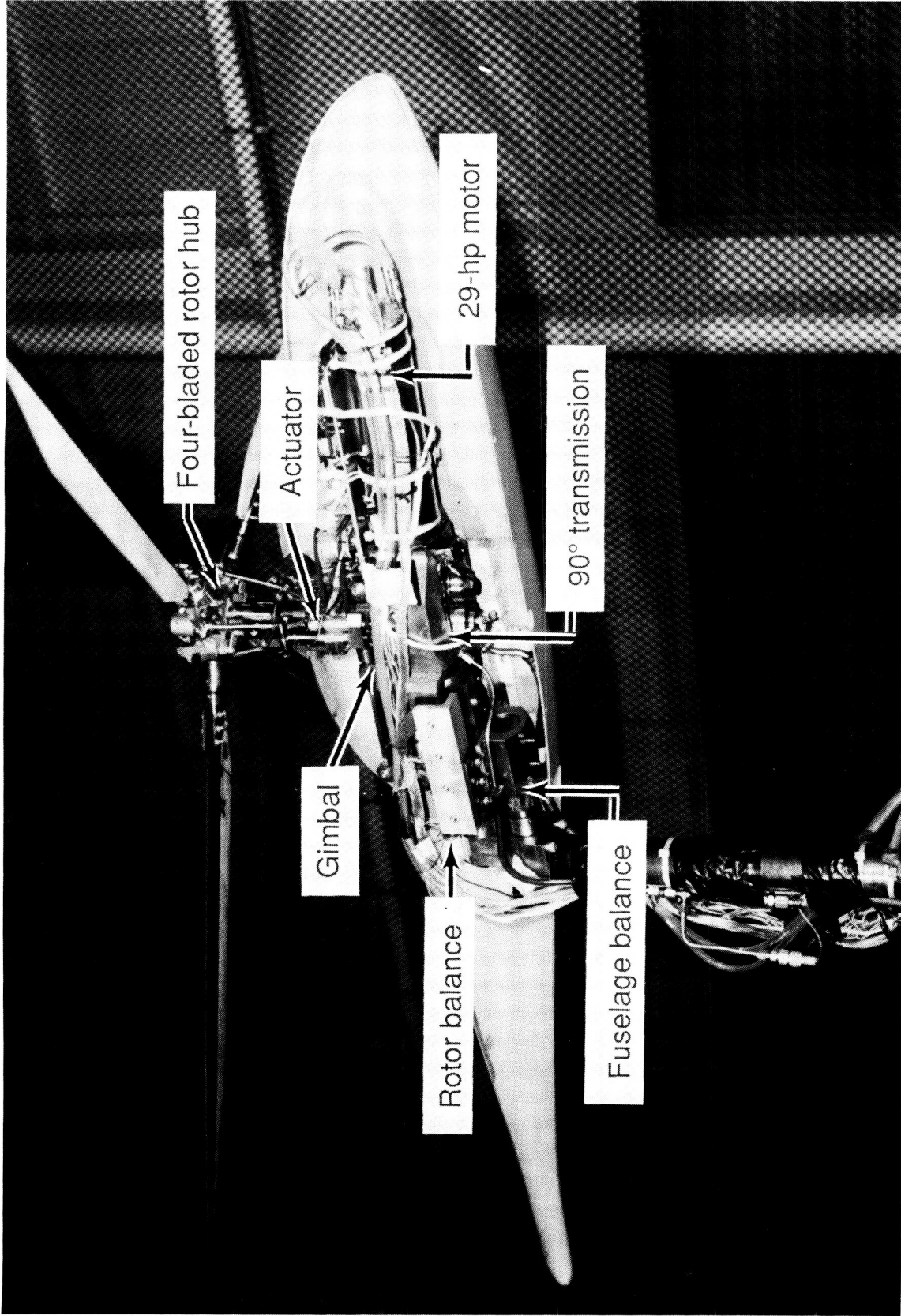


L-87-2896

(a) Model mounted for testing.

Figure 2. Photograph of test configuration in rotor test cell.

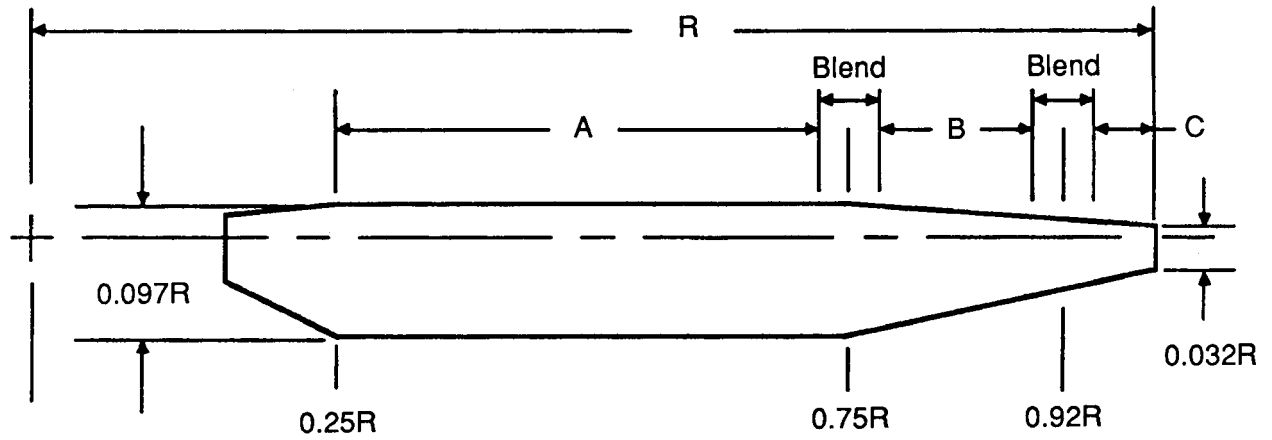
ORIGINAL PAGE  
BLACK AND WHITE PHOTOGRAPH



L-88-105

(b) Cutaway view of 2MRTS.

Figure 2. Concluded.



Blade	Twist, deg	R, in.	Airfoil		
			A	B	C
Baseline	-13	32.5	0012	0012	0012
Advanced	-13	32.5	RC(4)-10	RC(3)-10	RC(3)-08

Figure 3. Description of rotor-blade planform and airfoil distribution. Smooth transitions were accomplished between airfoils.

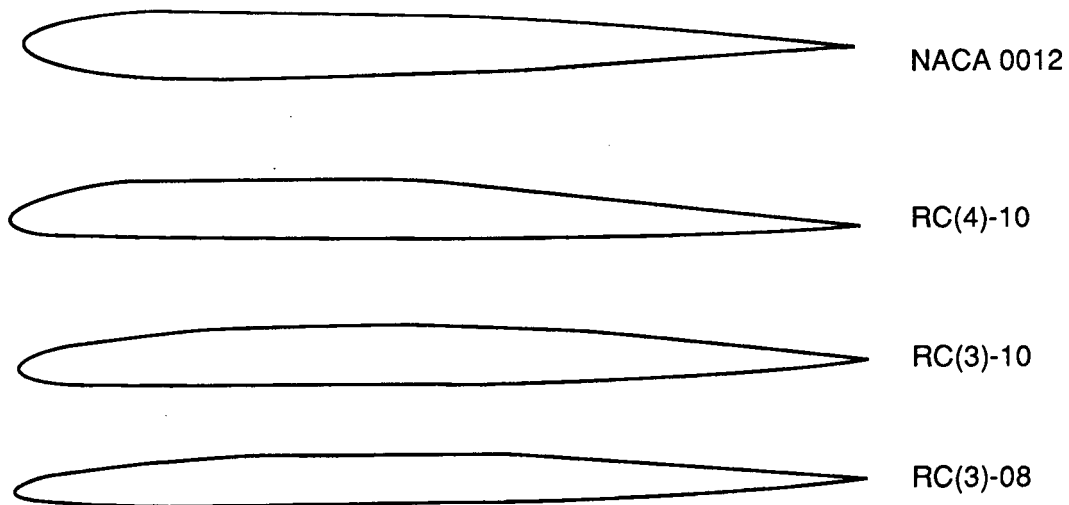


Figure 4. Profiles of rotor-blade airfoils.

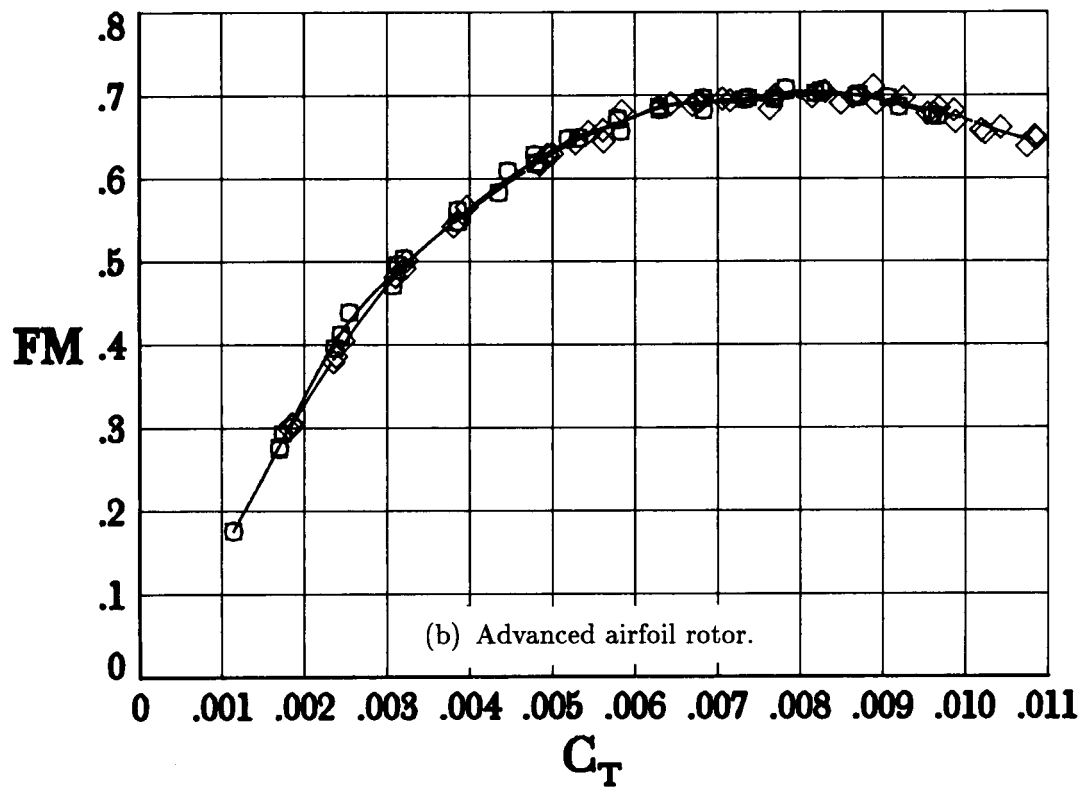
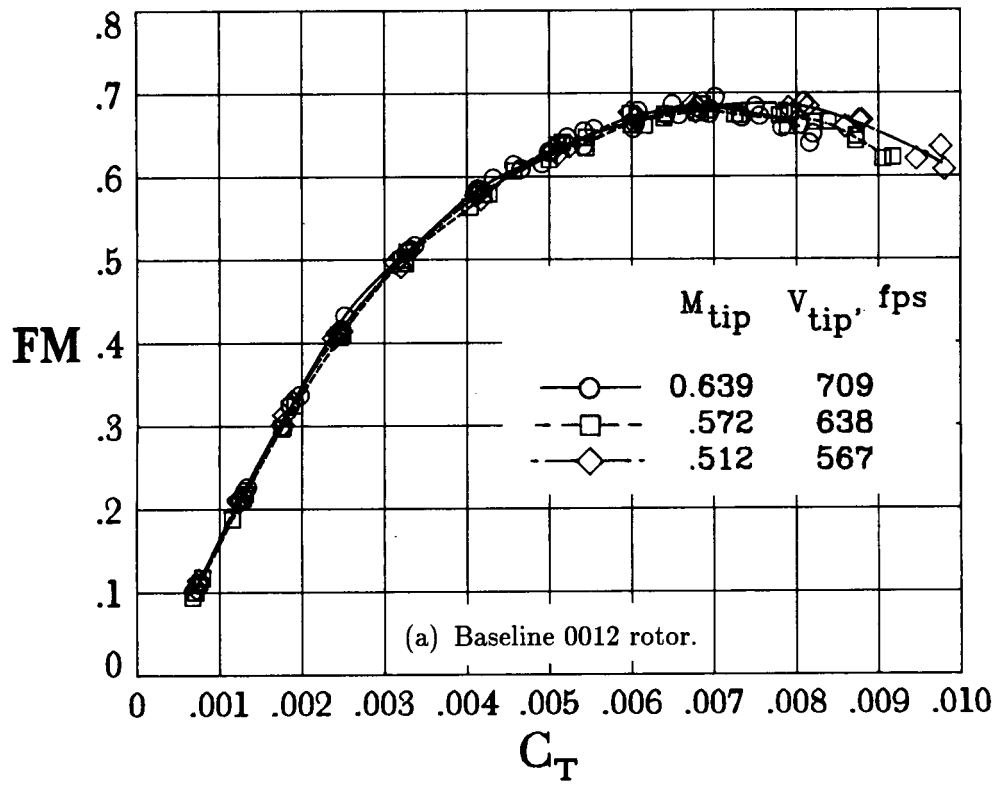


Figure 5. Basic aerodynamic characteristics of rotors for several values of  $M_{tip}$ .

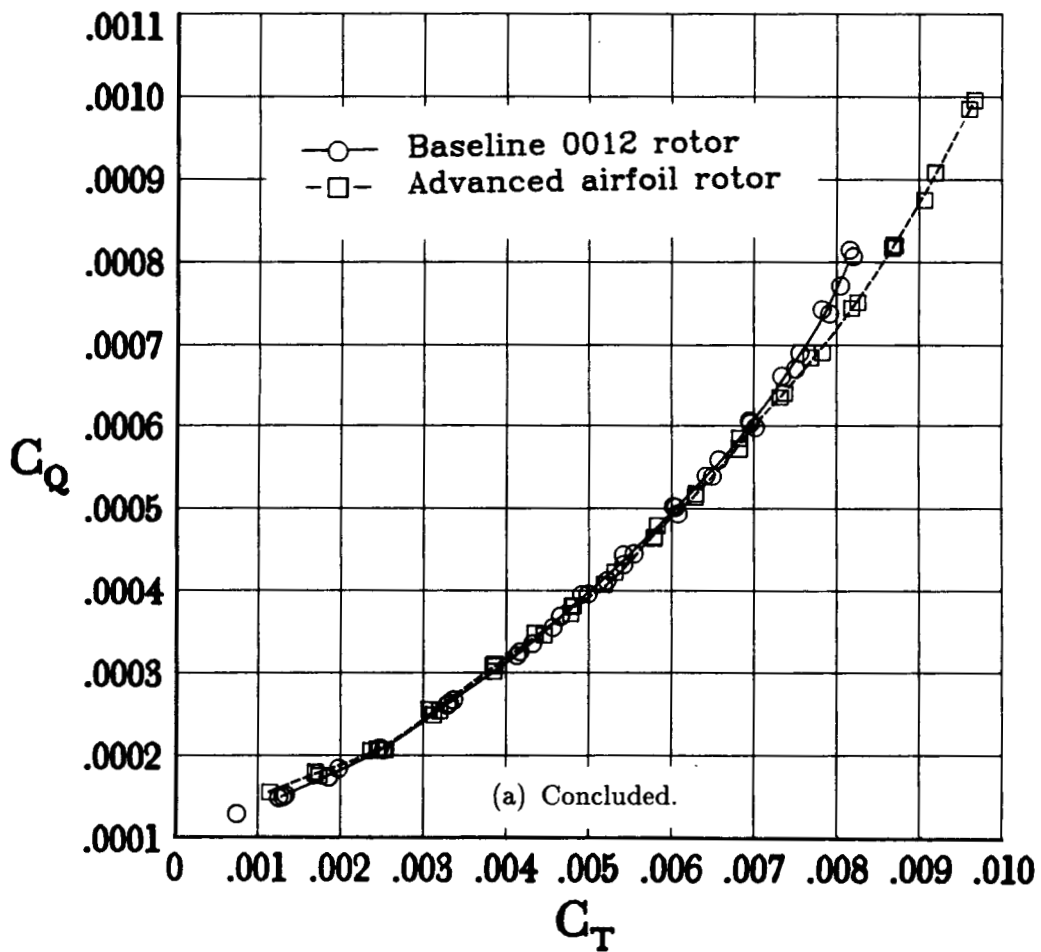
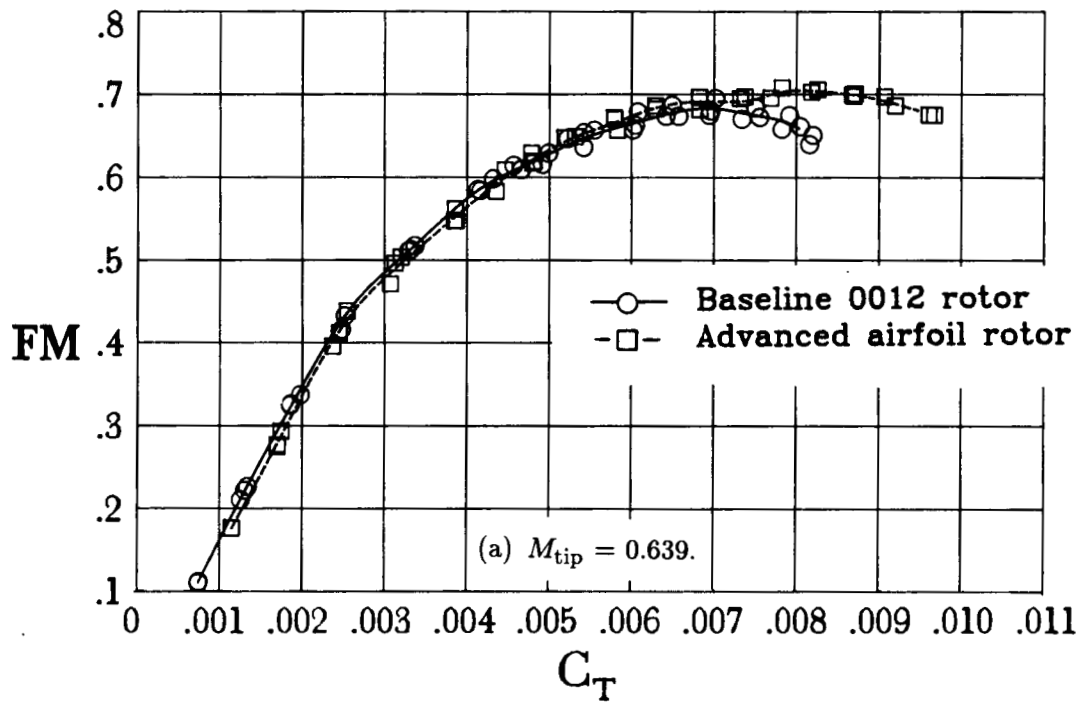


Figure 6. Comparison of aerodynamic characteristics of baseline and advanced rotors.

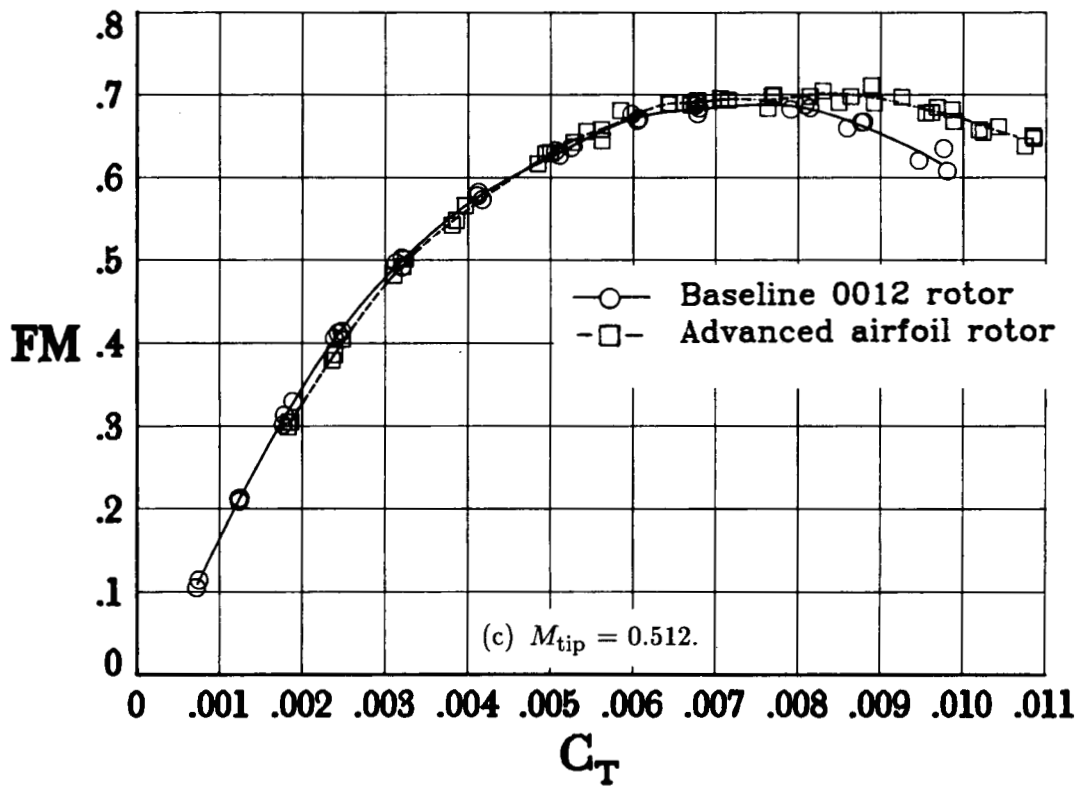
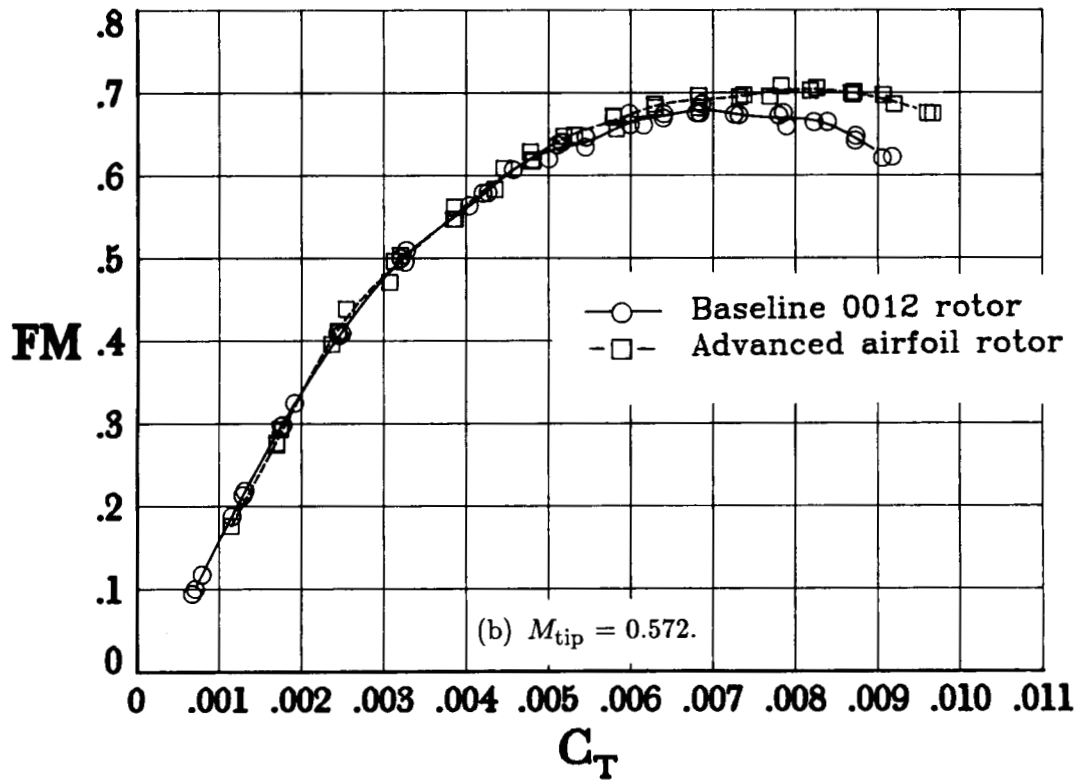


Figure 6. Continued.

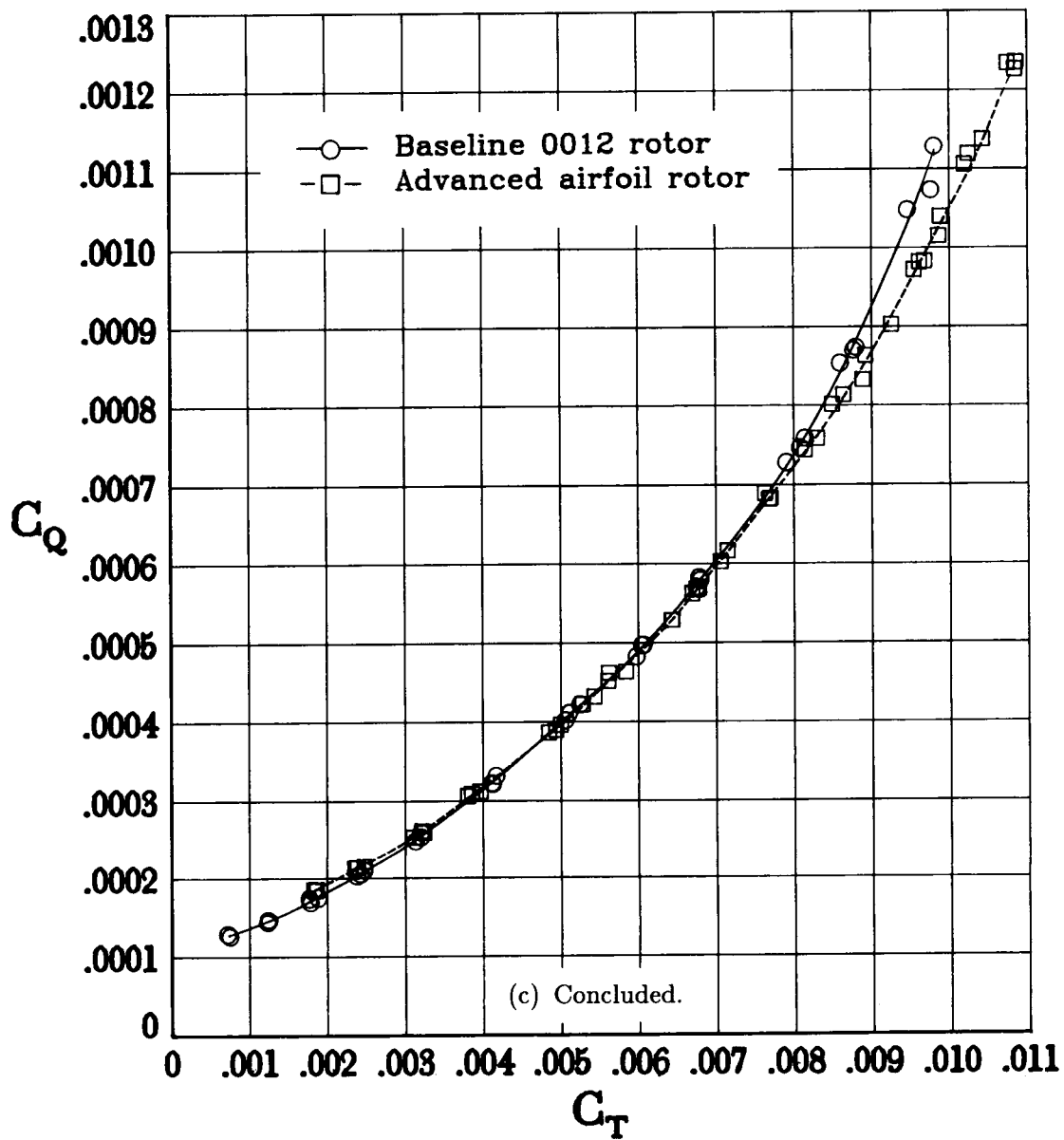


Figure 6. Concluded.

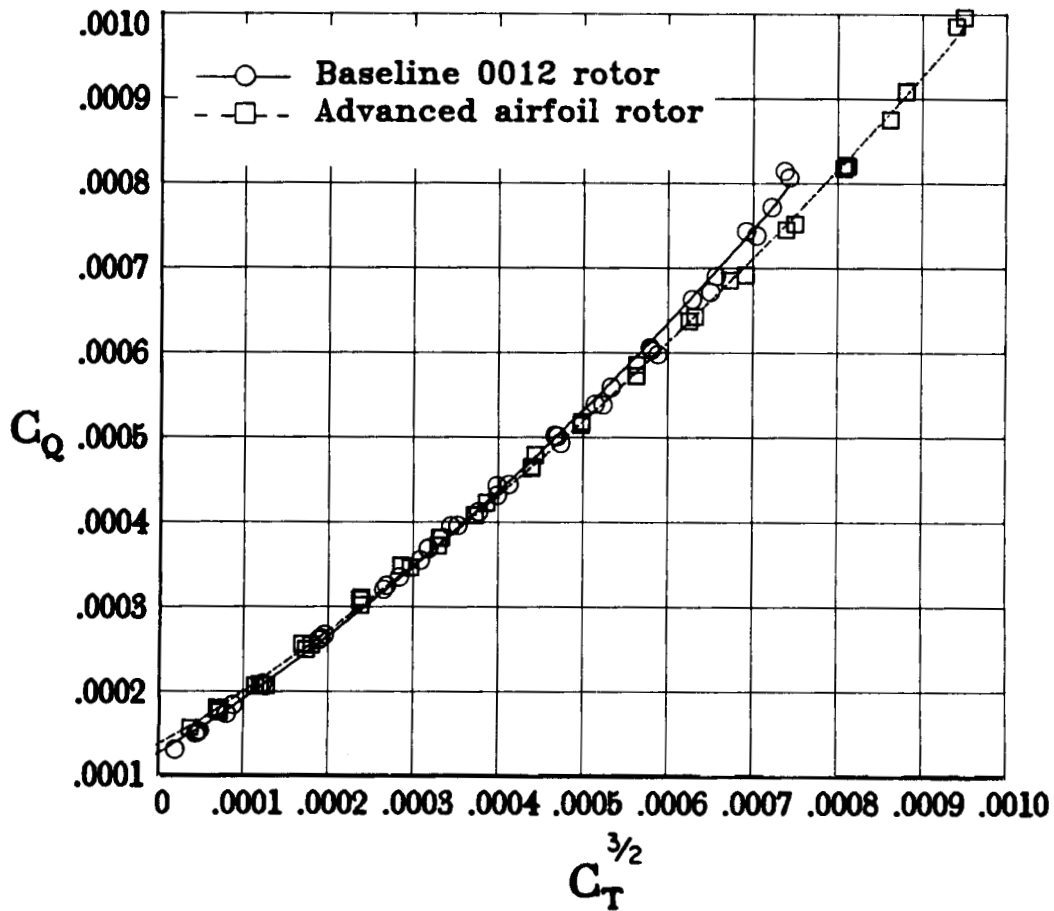


Figure 7. Power required to hover at  $M_{tip} = 0.639$ .

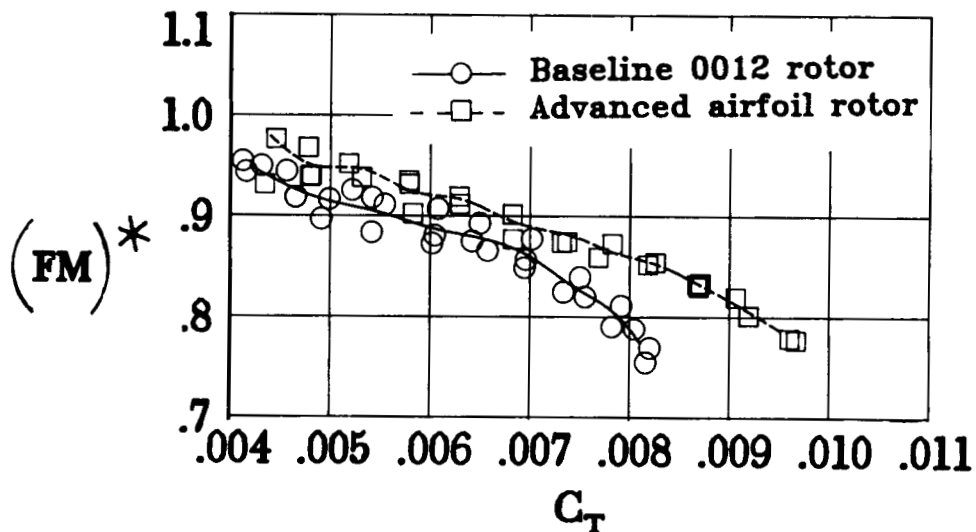


Figure 8. Comparison of alternate figure of merit for baseline and advanced airfoil rotors at  $M_{tip} = 0.639$ .

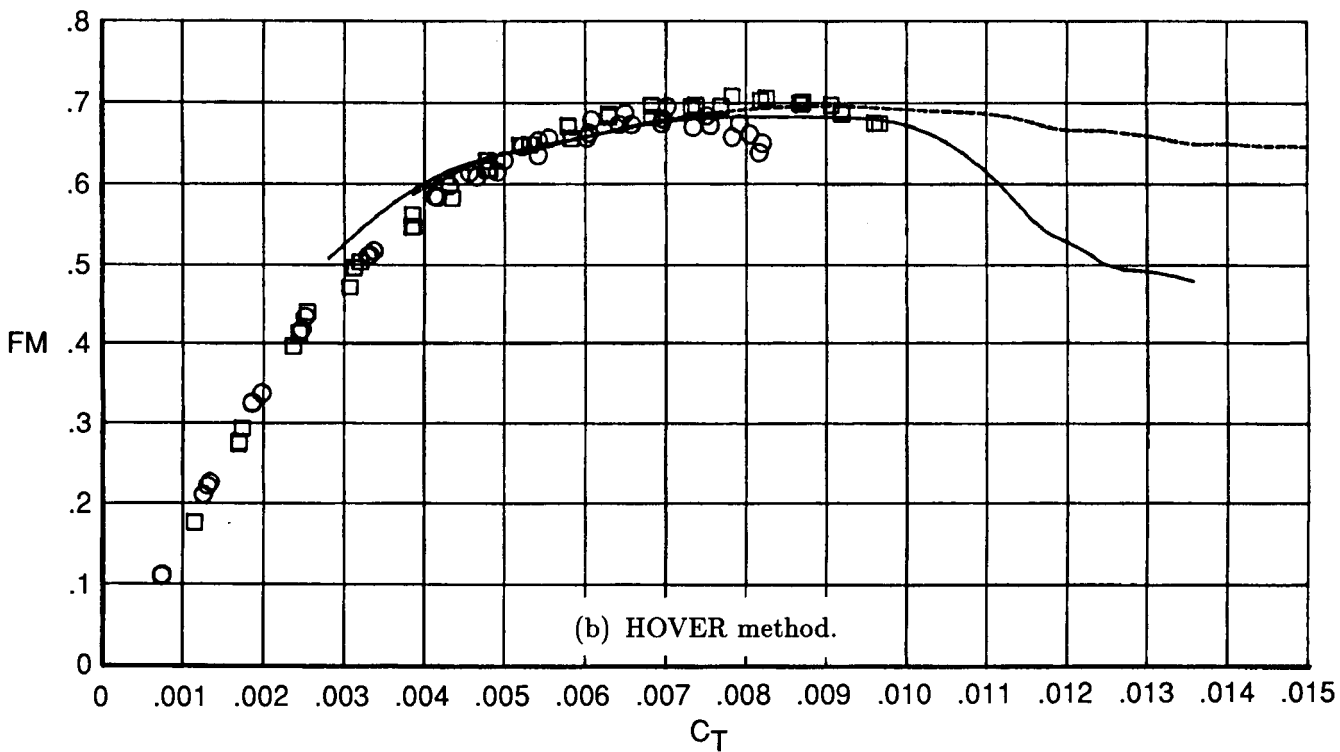
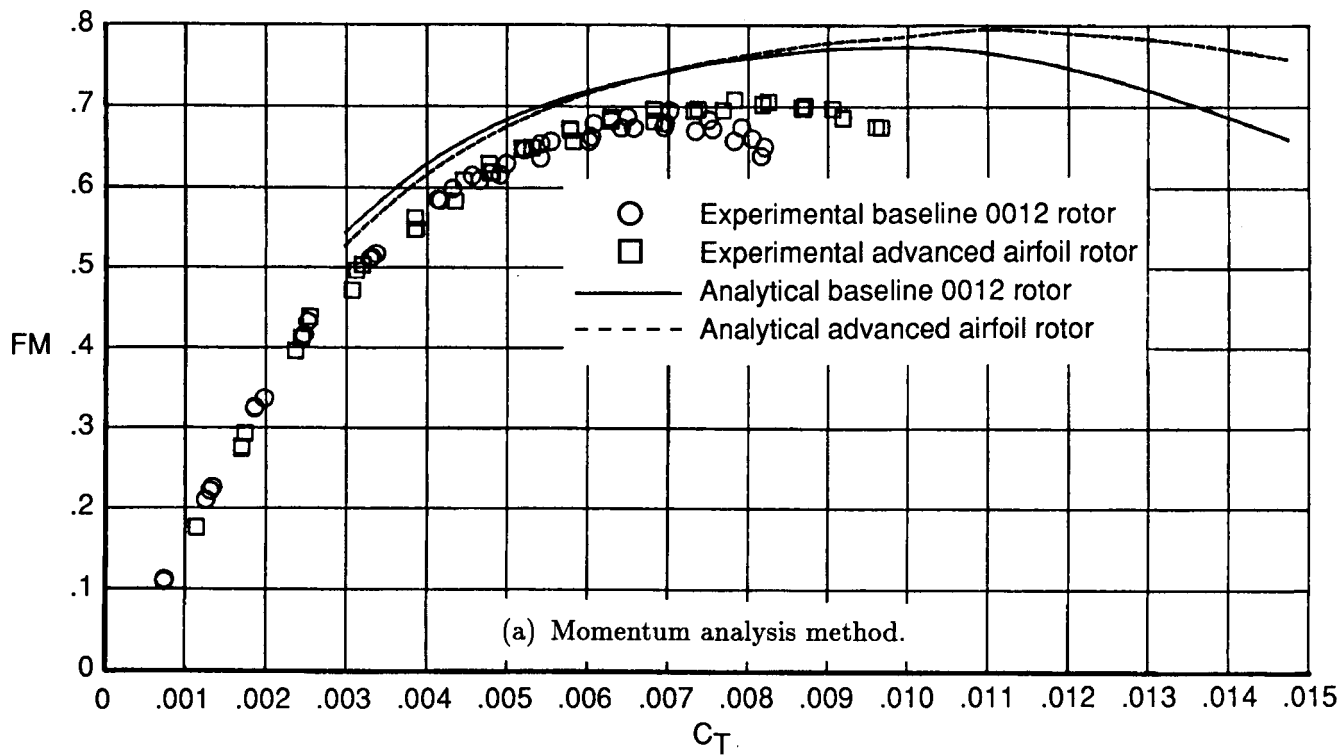


Figure 9. Comparison of prediction methods with experimental data at  $M_{tip} = 0.639$ .

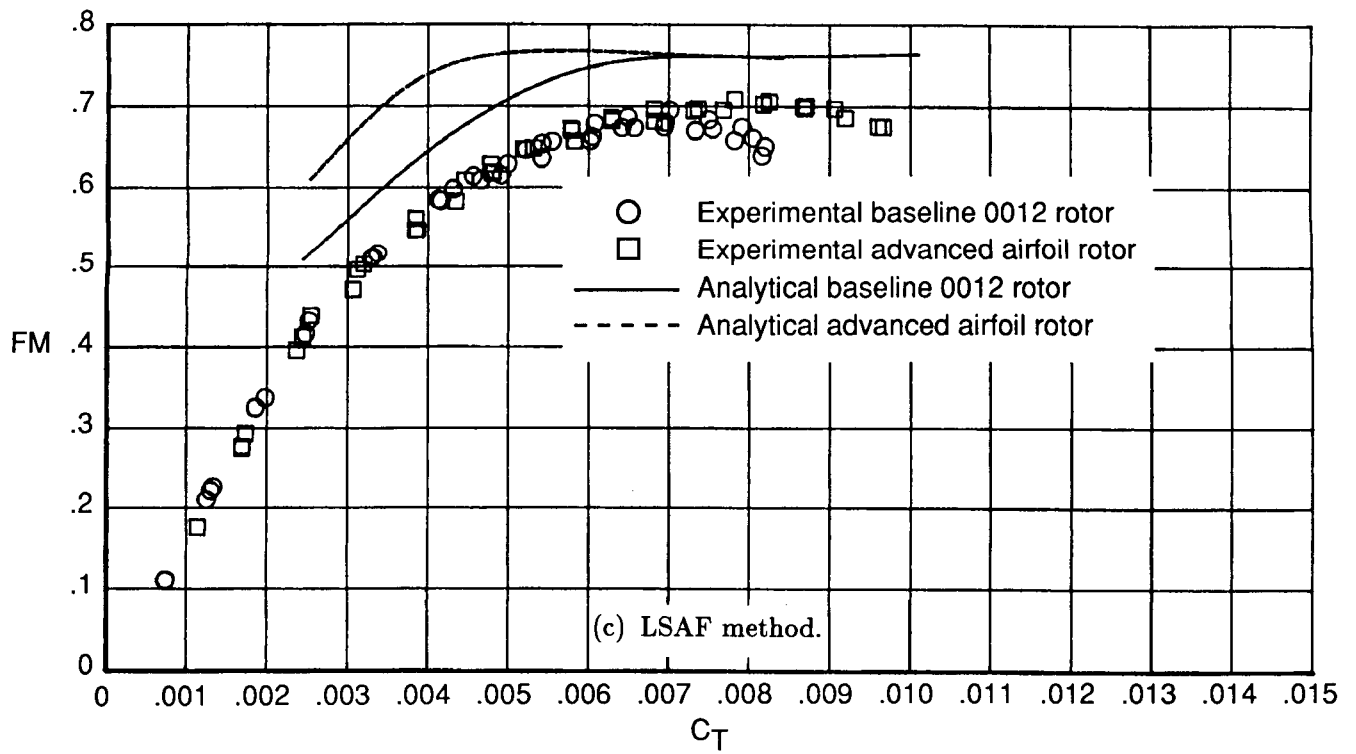


Figure 9. Concluded.

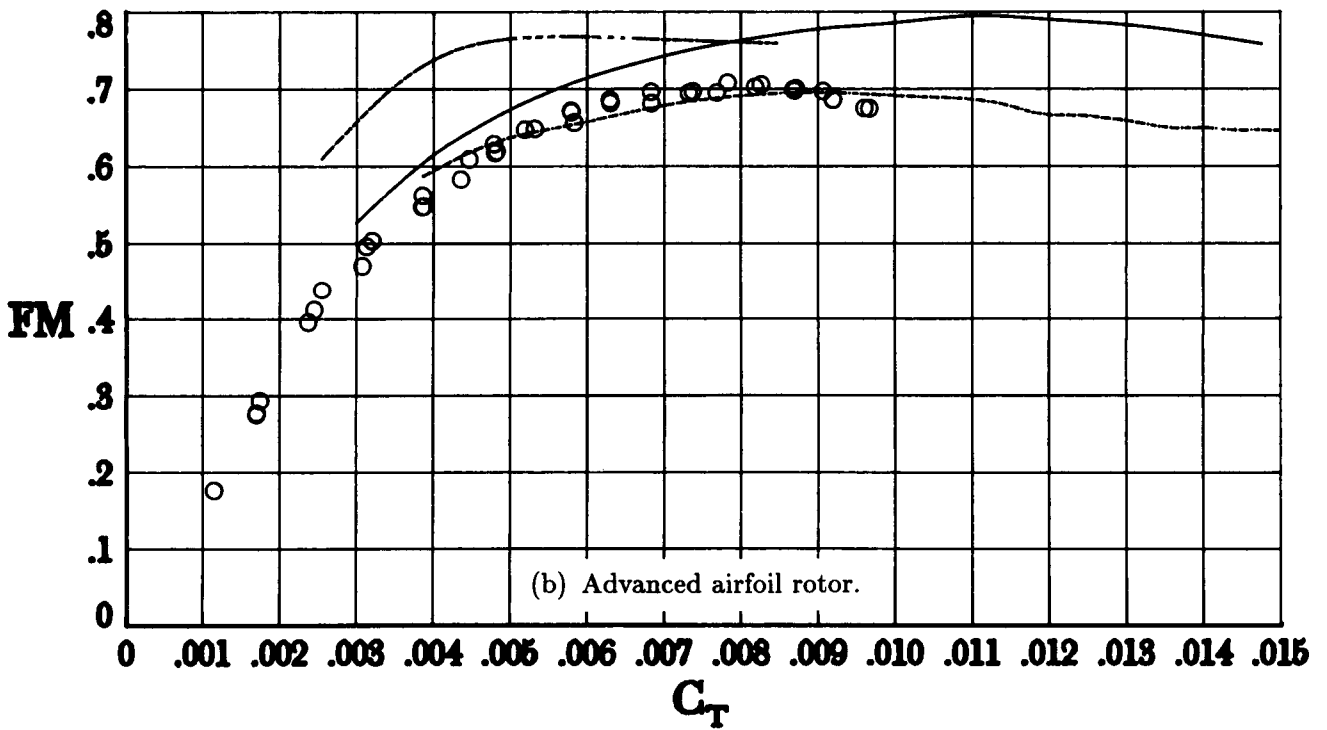
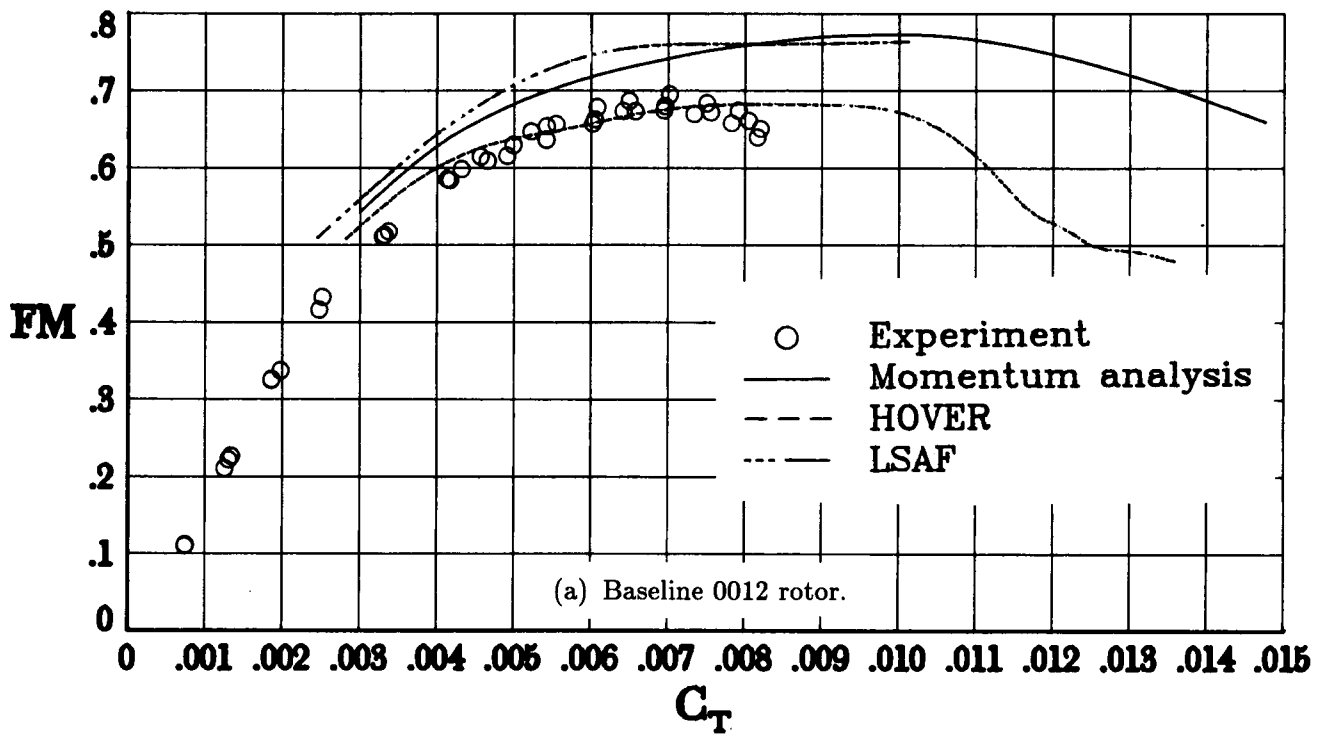


Figure 10. Comparison of three analytical methods at  $M_{tip} = 0.639$ .

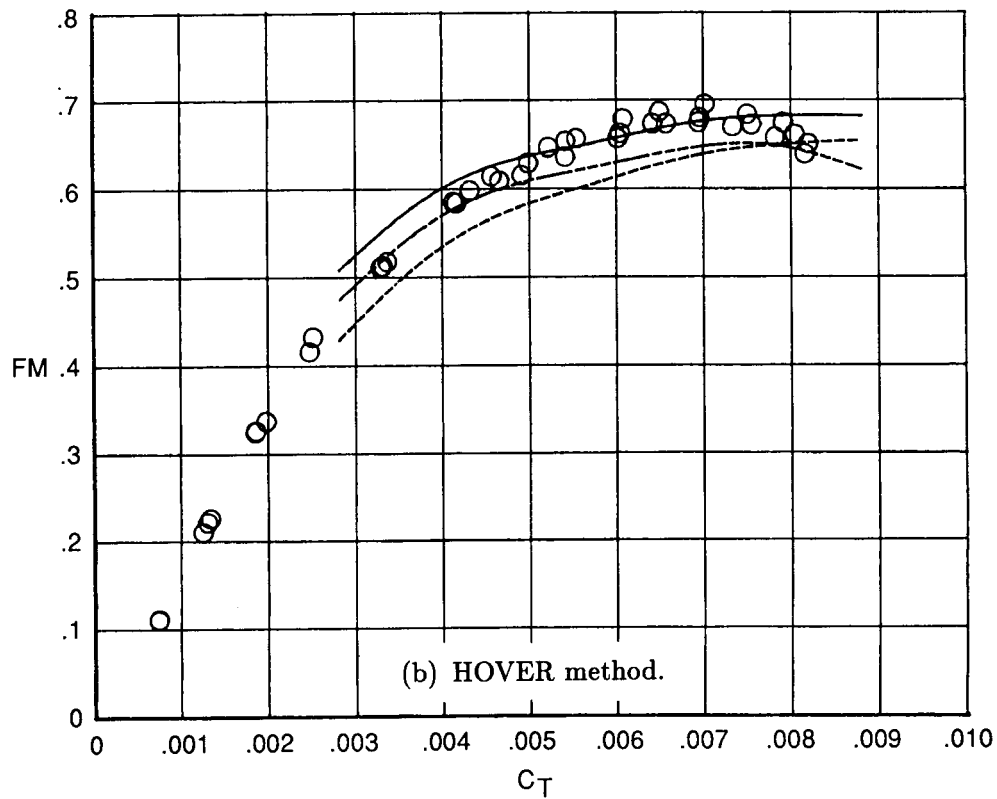
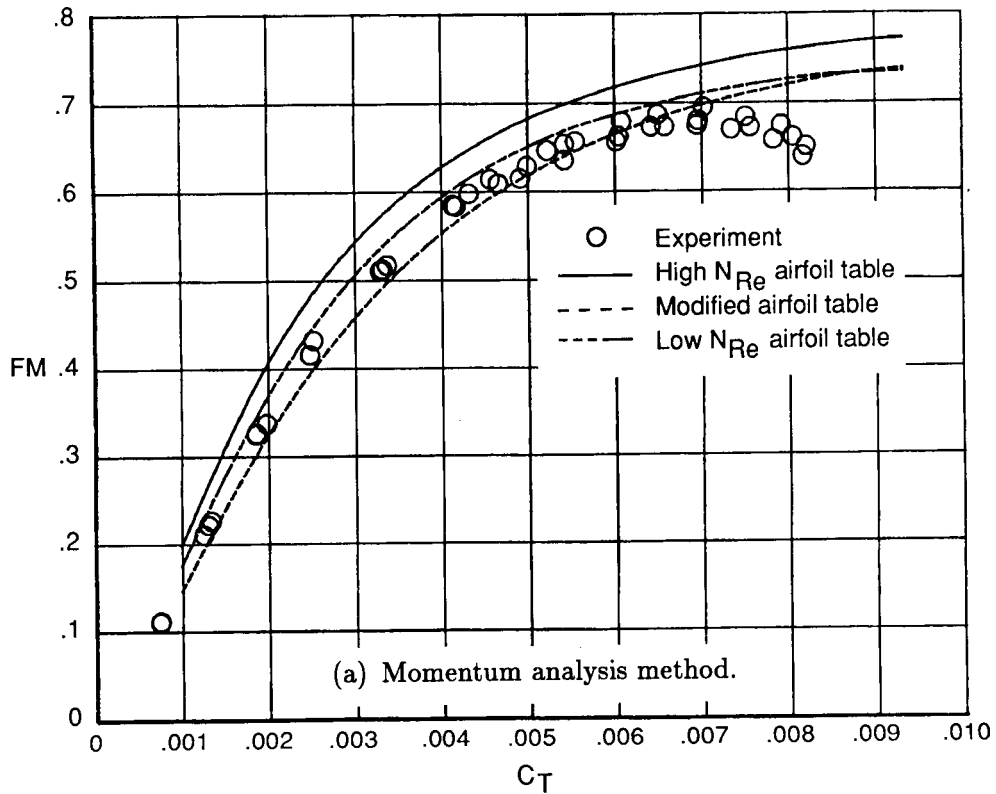


Figure 11. Effect of two-dimensional airfoil data tables on analytical results for baseline rotor at  $M_{tip} = 0.639$ .

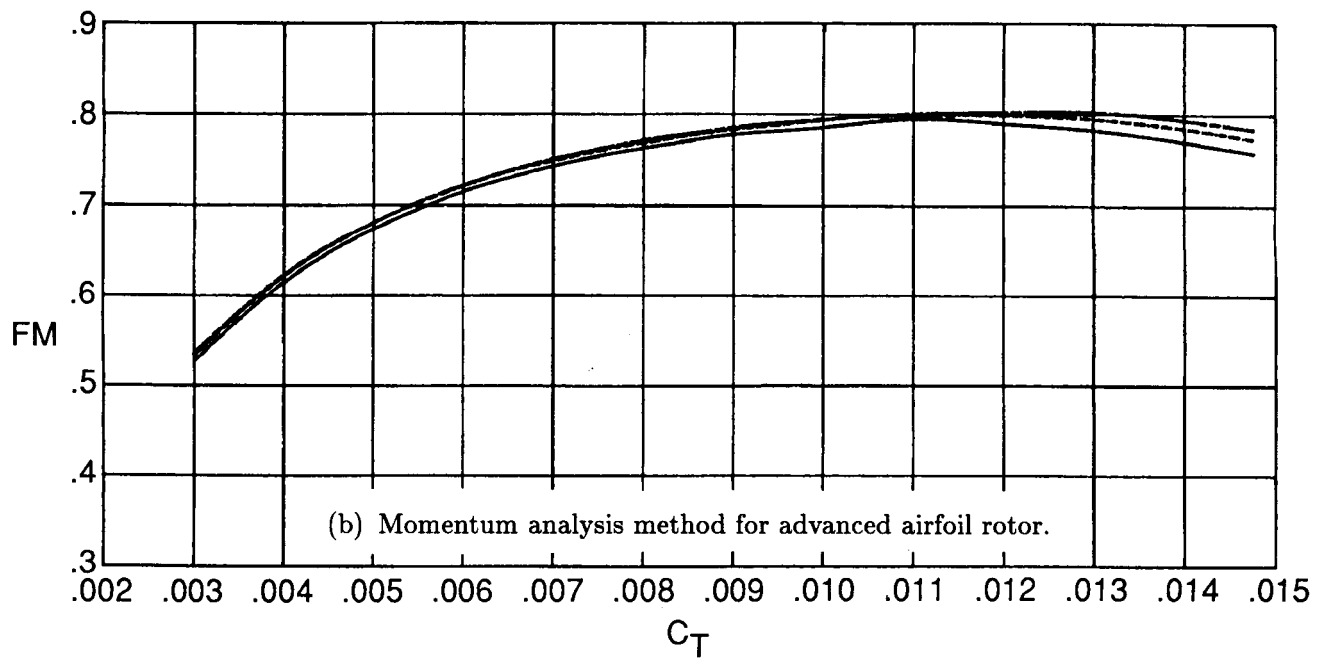
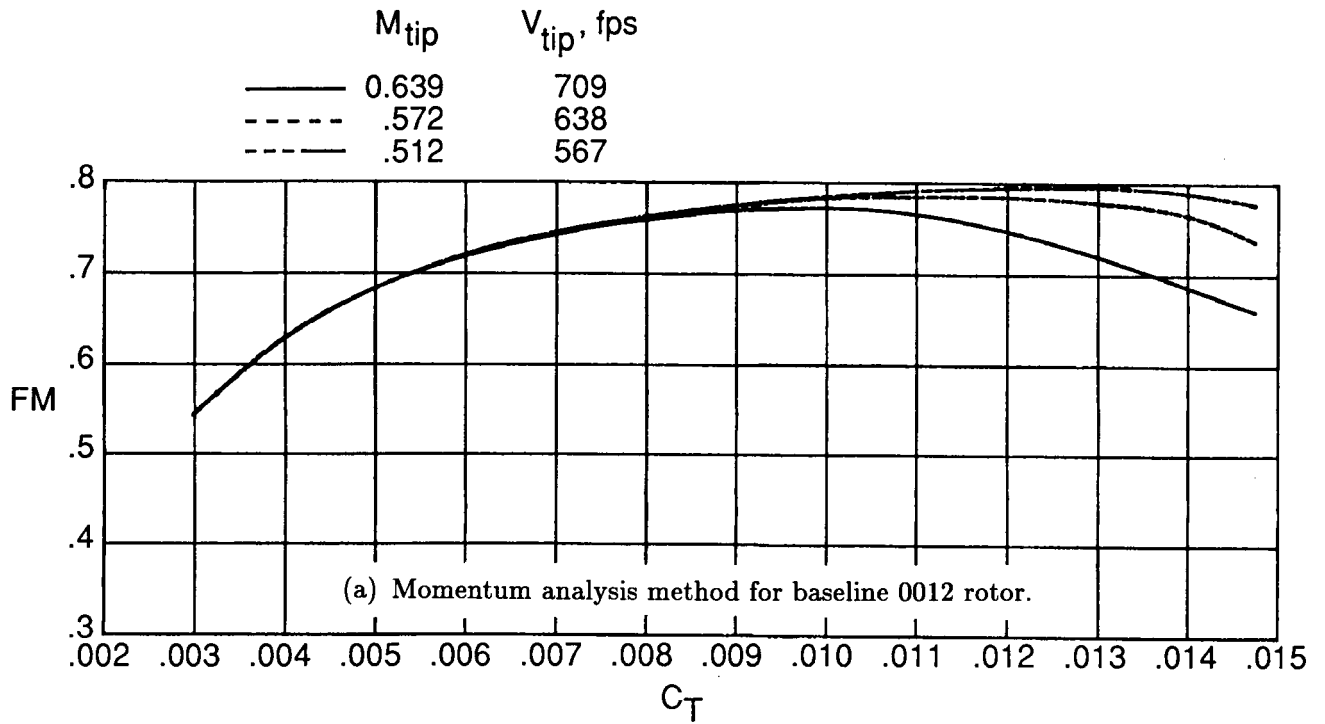


Figure 12. Comparison of analytical predictions for several values of  $M_{tip}$ .

	$M_{tip}$	$V_{tip}$ , fps
—	0.639	709
- - -	.572	638
- · -	.512	567

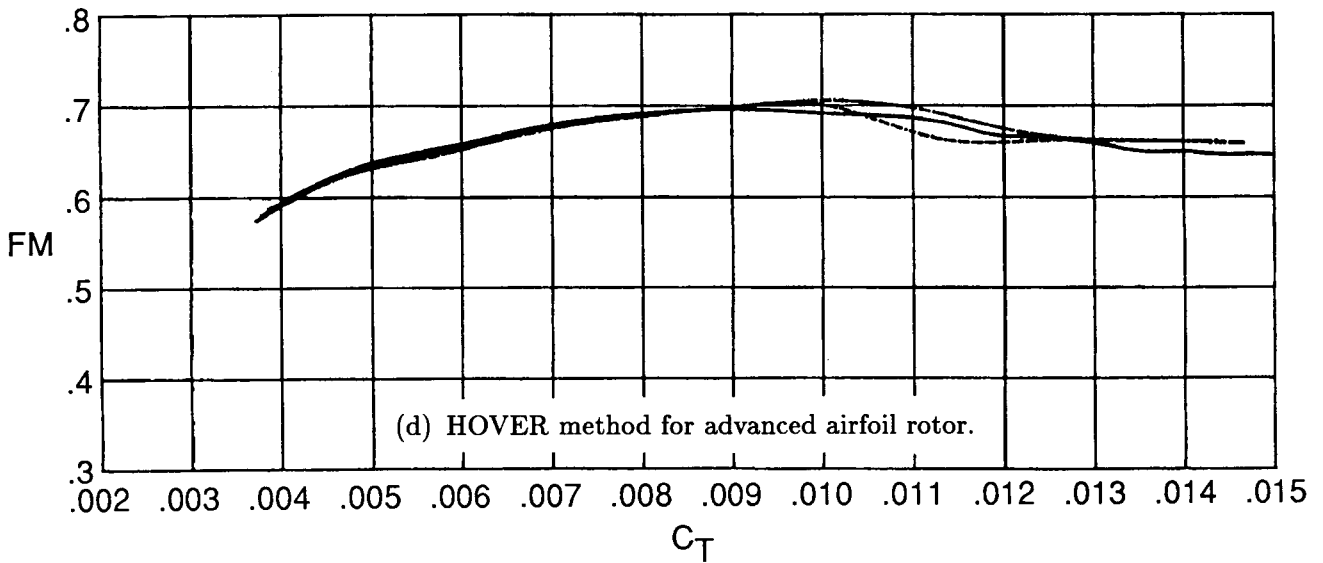
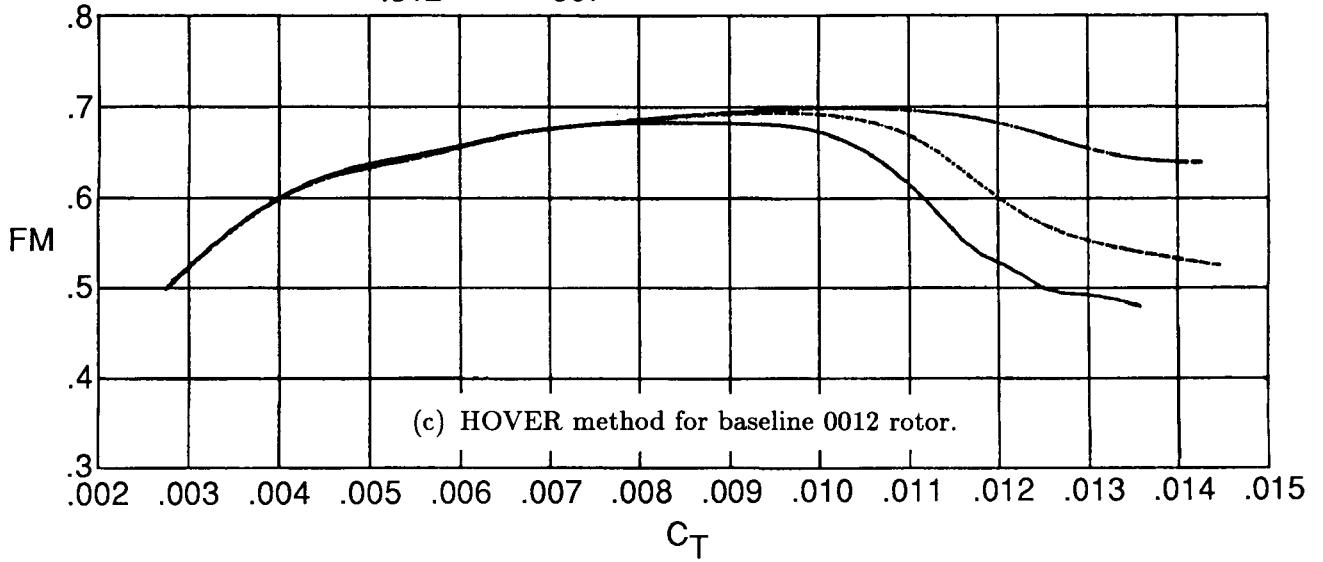
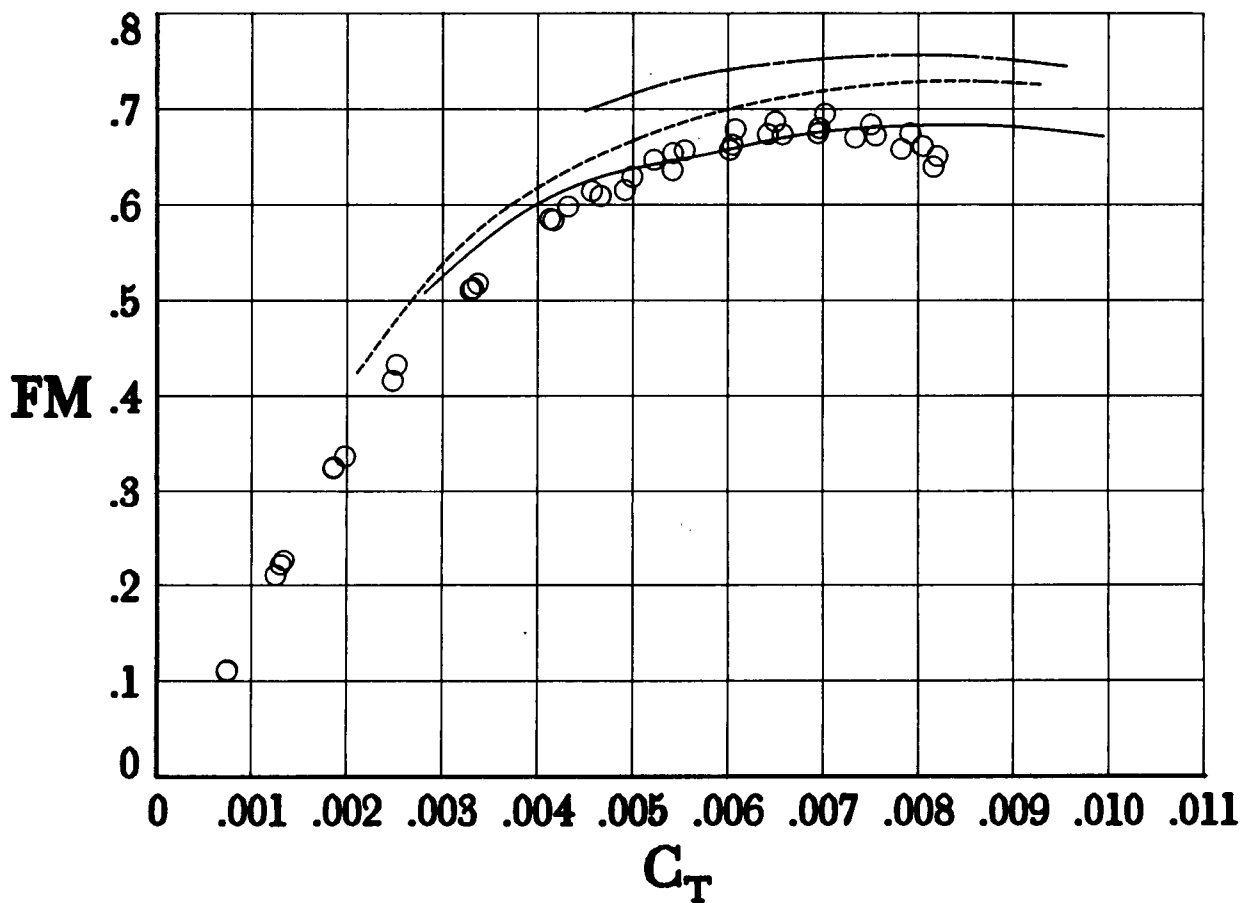


Figure 12. Concluded.

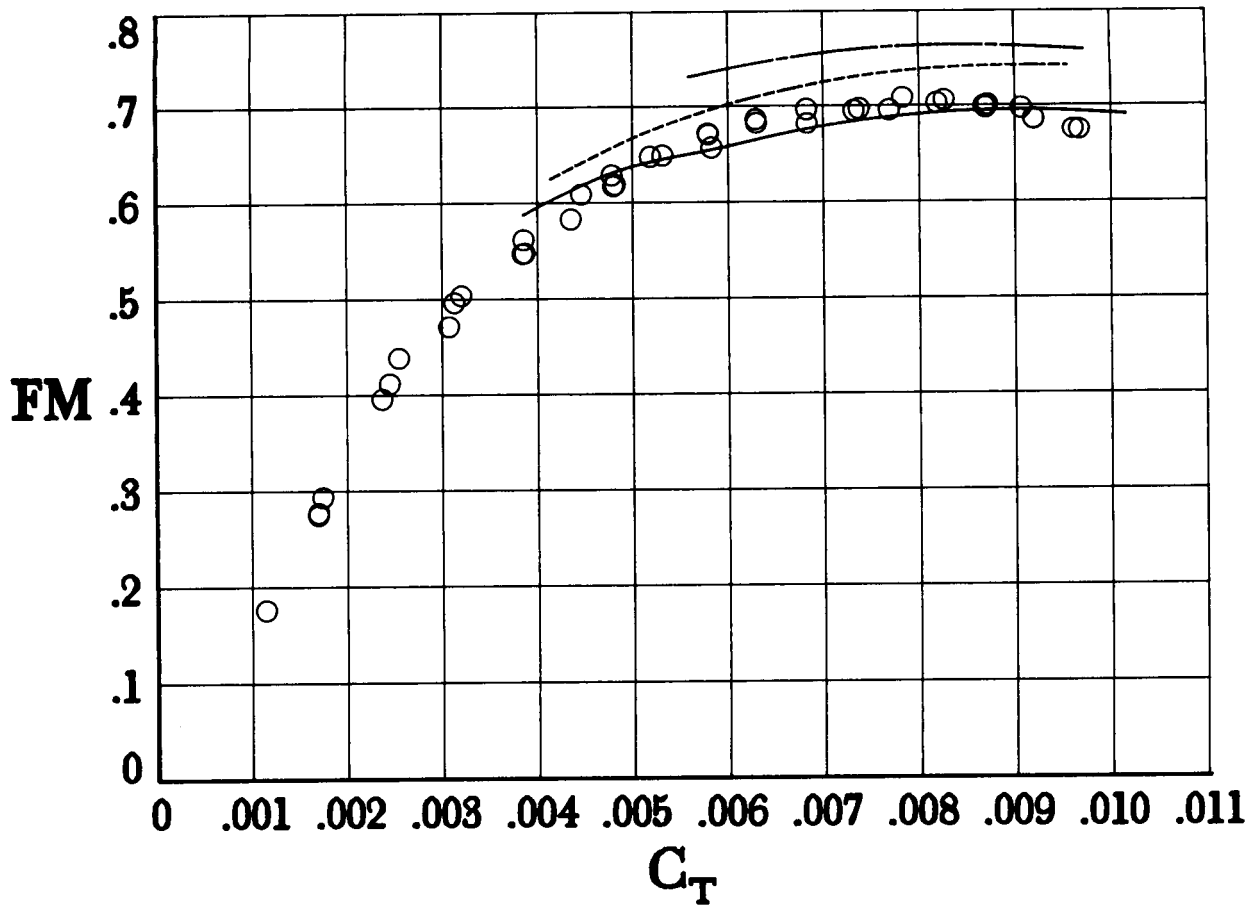
Calculation technique		
	Prescribed-wake portion	Free-wake portion
—	Based on momentum value	Internally calculated
- - -	0.75	0.75
- —	Internally calculated	Internally calculated
○	Experiment	



(a) Baseline 0012 rotor.

Figure 13. Effect of user input for radial position  $r/R$  of maximum circulation on performance calculations by HOVER at  $M_{tip} = 0.639$ .

Calculation technique		
	Prescribed-wake portion	Free-wake portion
—	Based on momentum value	Internally calculated
- - -	0.75	0.75
- —	Internally calculated	Internally calculated
○	Experiment	



(b) Advanced airfoil rotor.

Figure 13. Concluded.



## Report Documentation Page

1. Report No. NASA TP-2832 AVSCOM TP 88-B-001	2. Government Accession No.	3. Recipient's Catalog No.	
4. Title and Subtitle Effect of Advanced Rotorcraft Airfoil Sections on the Hover Performance of a Small-Scale Rotor Model		5. Report Date September 1988	6. Performing Organization Code
		8. Performing Organization Report No. L-16407	
7. Author(s) Susan L. Althoff		10. Work Unit No. 505-61-51-10	11. Contract or Grant No.
9. Performing Organization Name and Address Aerostructures Directorate USAARTA-AVSCOM Langley Research Center Hampton, VA 23665-5225		13. Type of Report and Period Covered Technical Paper	
		14. Army Project No. 1L161102AH45A	
12. Sponsoring Agency Name and Address National Aeronautics and Space Administration Washington, DC 20546-0001 and U.S. Army Aviation Systems Command St. Louis, MO 63120-1798		15. Supplementary Notes Susan L. Althoff: Aerostructures Directorate, USAARTA-AVSCOM, Hampton, Virginia.	
16. Abstract A hover test was conducted on a small-scale rotor model for two sets of tapered rotor blades. The baseline rotor-blade set used an NACA 0012 airfoil section, whereas the second rotor-blade set had advanced rotorcraft airfoils distributed along the radius. The experiment was conducted for a range of thrust coefficients and tip speeds, and the data were compared with the predictions of three analytical methods. The data show the advantage of the advanced airfoils at the higher rotor thrust levels; two of the analyses predicted the correct data trends.			
17. Key Words (Suggested by Authors(s)) Rotor Hover Rotorcraft airfoils		18. Distribution Statement Unclassified—Unlimited  Subject Category 02	
19. Security Classif.(of this report) Unclassified	20. Security Classif.(of this page) Unclassified	21. No. of Pages 33	22. Price A03